https://doi.org/10.5194/acp-2022-268
Preprint. Discussion started: 28 April 2022

Atmospheric Chemistry and Physics Discussions

Sources of organic aerosols in eastern China: A modeling study with high-resolution intermediate-volatility and semi-volatile organic compound emissions

Jingyu An[1], Cheng Huang[1*], Dandan Huang[1], Momei Qin[2,1], Huan Liu[3], Rusha Yan[1], Liping Qiao[1], Min Zhou[1], Yingjie Li[1], Shuhui Zhu[1], Qian Wang[1], Hongli Wang[1]

1. State Environmental Protection Key Laboratory of the Formation and Prevention of Urban Air Pollution Complex, Shanghai Academy of Environmental Sciences, Shanghai 200233, China
2. Jiangsu Key Laboratory of Atmospheric Environment Monitoring and Pollution Control, Collaborative Innovation Center of Atmospheric Environment and Equipment Technology, Nanjing University of Information Science & Technology, Nanjing 210044, China
3. State Key Joint Laboratory of Environment Simulation and Pollution Control, School of Environment, Tsinghua University, Beijing 100084, China

Abstract: Organic aerosol (OA) makes up a substantial fraction of atmospheric particulate matter that exerts tremendous impacts on air quality, climate, and human health. Yet current chemical transport models fail to reproduce both the concentrations and temporal variations of OA, especially the secondary organic aerosol (SOA), hindering the identification of major contribution sources. One possibility is that precursors that are not yet included in the model exist, and intermediate-volatility and semi-volatile organic compounds (I/SVOCs) are advocated to be one of them. Herein, we established a high-resolution emission inventory of I/SVOCs and by incorporating it into the CMAQ model, concentrations, temporal variations, and spatial distributions of POA and SOA originated from different sources in the Yangtze River Delta (YRD) region of China were successfully simulated. Compared with the comprehensive observation data obtained in the region, i.e., volatile organic compounds (VOCs), organic carbon (OC), primary organic aerosol (POA) and SOA, significant model

* Correspondence to C. Huang (huangc@saes.sh.cn)

https://doi.org/10.5194/acp-2022-268
Preprint. Discussion started: 28 April 2022


Atmospheric Chemistry and Physics Discussions

improvements in the simulations of different OA components were demonstrated. Furthermore, spatial and seasonal variations of different source contributions to OA production were identified. We found cooking emissions are predominant sources of POA in the densely populated urban area of the region. I/SVOC emissions from industrial sources are dominant contributors to the SOA formation, followed by those from mobile sources. While the former concentrated in eastern, central, and northern YRD, the latter mainly focused on the urban area. Our results indicate that future control measures should be specifically tailored on intraregional scale based on the different source characteristics to achieve the national goal of continuous improvement in air quality. In addition, local source profiles and emission factors of I/SVOCs as well as SOA formation mechanisms in model framework are urgently needed to be updated to further improve the model performance and thus the accuracy of source identifications.
Key words: semi-volatile and intermediate volatility organic compounds; secondary organic aerosol; emission inventory; source contribution; model simulation

1. Introduction

Organic aerosol (OA) contributes a large fraction (20 to 90%) of atmospheric submicron aerosol (Zhang et al., 2007; Jimenez et al., 2009) and has negative impacts on air quality, climate (Shrivastava et al., 2017), and human health (Nault et al., 2021). OA is composed of primary organic aerosol (POA) directly emitted from fossil fuel combustion, biomass burning, and other sources, as well as secondary organic aerosol (SOA) formed through the atmospheric oxidation of gas-phase species emitted from a wide range of biogenic and anthropogenic sources (Hallquist et al., 2009). Understanding and identifying the origins of OA is therefore important for elucidating their health and climate effects and establishing effective mitigation policies. However, OA is a dynamic system driven by the gas-particle partitioning of organic vapors and particulate organic material, i.e. POA and SOA, and continuously evolves upon atmospheric oxidation (Robinson et al., 2007; Donahue et al., 2009; Zhao et al., 2013; Jathara et al., 2014). Constraints in their precursors and further source identification

https://doi.org/10.5194/acp-2022-268
Preprint. Discussion started: 28 April 2022


Atmospheric Chemistry and Physics Discussions

have been facing great challenges.

Great efforts have been made in the identification of OA sources through source apportionment of the measured OA components, such as positive matrix factorization (PMF), chemical mass balance (CMB) model or multilinear engine (ME-2). The Aerodyne high-resolution time-of-flight aerosol mass spectrometer (AMS), has been proven to be a powerful tool in quantification and chemical characterization of different OA components in real-time. Coupled with PMF analysis, AMS measurements allow for the deconvolution of physically meaningful OA factors. Commonly retrieved factors include three POA sources, i.e. hydrocarbon-like OA (HOA) related to fossil fuel combustion, biomass burning OA (BBOA), and cooking-related OA (COA), as well as two SOA components, i.e. less oxidized oxygenated OA (LO-OOA) and more oxidized oxygenated OA (MO-OOA) (Hayes et al., 2013; Crippa et al., 2014; Sun et al., 2014; Li et al., 2017). Combining offline AMS and radiocarbon (^{14}C) measurements, Huang et al. (2014) also identified the contributions of fossil and non-fossil sources to SOA. Attempts have been made in subsequent studies by coupling the AMS measurement with a suite of comprehensive and collocated SOA tracer measurements to distinguish biogenic and major anthropogenic SOA sources, such as traffic and cooking emission (Xu et al., 2015; Zhang et al., 2018; Zhu et al., 2020; Huang et al., 2021a). However, due to the complex OA composition and variety of emission sources, further deconvolution on the contributions of different sources to OA production is challenging.

Besides field measurements, air quality model is another widespread technique, which advantages in regional-scale OA source apportionment with higher temporal and spatial resolution. However, the model simulated SOA concentration is substantially lower than that measured in the atmosphere. On one hand, this is limited by the model treatment, where multiple-generation oxidation of organic vapors is not included. The volatility basis set (VBS) scheme is therefore developed, which lumps organic precursors as well as their oxidation products into different volatility bins. Upon atmospheric aging, the volatility of these compounds evolves due to the processes such

https://doi.org/10.5194/acp-2022-268
Preprint. Discussion started: 28 April 2022


Atmospheric Chemistry and Physics Discussions

as functionalization and fragmentation, which can be accounted for in the models by shifting the volatility bins of these compounds (Donahue et al., 2006). It has been widely reported that coupling VBS scheme with air quality models can improve the model performance on SOA simulation (Tsimpidi et al., 2010; Koo et al., 2014; woody et al., 2016; Zhao et al., 2016a; Yang et al., 2019). On the other hand, the gaps are still not closed mainly due to the missing of intermediate-volatility organic compounds (IVOCs) and semi-volatile organic compounds (SVOCs) emissions in the models, which potentially have substantial contributions to SOA budget owing to their high SOA yields (Presto et al., 2009; Tkacik et al., 2012; Zhao et al., 2014; Liggio et al., 2016). However, due to the vast number of different I/SVOC components with low volatility (C* of 10^{-1} to 10^{6} $\mu g \cdot m^{-3}$) and concentrations, qualitative and quantitative characterization of I/SVOCs in molecular level are difficult. Recent studies have successively determined the volatility distribution, chemical composition, and emission factors of I/SVOCs from mobile sources, including gasoline and diesel vehicles, non-road diesel machinery, marine vessel, and aircraft (Presto et al., 2011; Cross et al., 2013; Zhao et al., 2015, 2016b; Huang et al., 2018; Qi et al., 2019; Drozd et al., 2019). I/SVOC emission profiles have been reported for nonmobile-sources as well, including coal combustion, wood-burning, cooking, fuel evaporation, and industrial and residential volatile chemical products (Huffman et al., 2009; Gentner et al., 2012; May et al., 2013; Koss et al., 2018; McDonald et al., 2018; Cai et al., 2019; Drozd et al., 2021). Most of these reported emission profiles have been released in SPECIATE 5.1 (US EPA, 2021), making the quantification of I/SVOC emissions and their involvement in air quality models possible.

In China, SOA has been emerging as an important contributor to air pollution. Field observations reveal that OA dominates (30%) the $PM_{2.5}$ concentrations in most parts of China (Tao et al., 2017; Liu et al., 2018), among which the SOA contributes up to 80% of OA during haze pollution (Huang et al., 2014; Ming et al., 2017; Li et al., 2021). SOA formation in China has already been examined in several modeling studies.

https://doi.org/10.5194/acp-2022-268
Preprint. Discussion started: 28 April 2022


Atmospheric Chemistry and Physics Discussions

They found that by considering the POA aging and I/SVOCs oxidation in the models, which is realized by the coupling of VBS scheme, the formation and evolution of SOA can be much better simulated compared to the results of the two-product SOA modeling framework (Zhao et al., 2016a; Wu et al., 2019; Li et al., 2020; Yao et al., 2020; Huang et al., 2021). However, large uncertainties still exist in the estimation of I/SVOC emissions used in previous modeling studies, which has essential impacts on model performance. Theoretically, the I/SVOC emissions can be obtained quantitatively by applying different scaling factors to POA emissions from different sources. Yet in practice, a same scaling factor was applied to most of the sources in previous studies due to the lack of measurements on I/SVOC emission factors. For example, except biomass burning (0.75–1.5), Wu et al. (2019) utilized scaling factors of 8–30 for all of the other emission source categories, which was estimated based on the measurements of on-road mobile source. Li et al. (2020) assumed scaling factors of 1.5 for on-road mobile source, and 0.34–1.5 for the other sources, such as industrial and residential sources, which were much lower than the estimations in Wu et al. (2020). Huang et al. (2021) have tried emission factor method to quantify the I/SVOC emissions, yet the results were 60% lower than the scaling factor method, far from catching the measured amount of SOA.

Beyond the aforementioned uncertainties, another obstacle is that I/SVOC emission profiles have not been taken into account in previous studies. It should be noted that volatility and chemical composition of I/SVOC emissions vary by source category (Lu et al., 2018), which matters in model simulation because different I/SVOC components are of different SOA yields. For example, the SOA yields of *n*-alkanes increase with increasing carbon number (Presto et al., 2010) and for a given volatility bin, the aromatics usually have higher SOA yields than the alkanes (Lim and Ziemann, 2009; Tkacik et al., 2012). In a recent study, Lu et al. (2020) compiled new emission profiles for I/SVOCs based on the existing mobile-source emission data and incorporated them into an updated version of the Community Multiscale Air Quality

https://doi.org/10.5194/acp-2022-268
Preprint. Discussion started: 28 April 2022


Atmospheric Chemistry and Physics Discussions

model version 5.3 (CMAQ v5.3) to investigate their contributions to SOA formation. Their results indicated that mobile-source related I/SVOC emissions produced almost as much SOA as traditional precursors such as single-ring aromatics in southern California and suggested that the potential contributions of nonmobile-source I/SVOC emissions were nonnegligible to SOA formation (Lu et al., 2020).

In this study, taking the Yangtze River Delta (YRD) region, including Jiangsu, Zhejiang, Anhui provinces and Shanghai city, as a pilot, we established a high-resolution source specific I/SVOC emission inventory. We then applied the newly established inventory into CMAQ v5.3 to evaluate the contributions of I/SVOC emissions to SOA formation by comparing the results with the observation data collected in the region. Furthermore, we also run the model in different scenarios to quantify the seasonal contributions of different sources to POA and SOA formation in the YRD region.

2. Materials and methods

2.1 I/SVOC emission estimates

I/SVOCs commonly exist in both gas- and particle-phase in the atmosphere. Herein, we compiled both gas-phase I/SVOCs (I/SVOCs-G) and particle-phase I/SVOCs (I/SVOCs-P) emission inventories and incorporate them into the model. I/SVOCs-G emissions for each specific source were estimated by the ratios of total I/SVOC components to VOC components (I/SVOCs-to-VOCs). Similarly, I/SVOCs-P emissions were estimated by the ratios of total particle-phase I/SVOC components to POA (I/SVOCs-to-POA). On this basis, we further determined the source profiles of I/SVOCs for each source. The I/SVOCs-G emissions were distributed into four lumped aliphatic IVOC bins across the volatility basis set from $C^*=10^3$ to 10^6 $\mu g \cdot m^{-3}$, two aromatic IVOC bins with the $C^*=10^5$ and 10^6 $\mu g \cdot m^{-3}$, and four lumped SVOC bins with C^* from 10^{-1} and 10^2 $\mu g \cdot m^{-3}$. The I/SVOCs-P emissions were distributed into five bins spanning C^* from 10^{-1} and 10^3 $\mu g \cdot m^{-3}$.

In this study, we first divided the sources into five categories, including industrial

https://doi.org/10.5194/acp-2022-268
Preprint. Discussion started: 28 April 2022


Atmospheric Chemistry and Physics Discussions

process sources, industrial solvent-use sources, mobile sources, residential sources, and agricultural sources, and then further grouped them into 21 sub-categories. For example, industrial process sources include the sectors such as oil refinery, chemical production, and pulp and paper production; Industrial solvent-use sources include textile, leather tanning, timber processing, and various industrial volatile chemical products use; Mobile sources include gasoline and diesel vehicle emissions, fuel evaporation, diesel machinery, marine vessel, and aircraft; Residential sources include coal combustion, residential solvent-use, and cooking emissions; Agricultural source is specifically referred to biomass burning in household stoves, and open burning was not included in this study. For gasoline and diesel vehicles, the I/SVOCs-G-to-VOCs and I/SVOCs-P-to-POA ratios and their emission profiles were derived from a new mobile-source parameterization recommended by Lu et al. (2020). Those of diesel machinery, marine vessel, and residential coal combustion were determined by recent measurement results in China (Qi et al., 2019; Huang et al., 2018; Cai et al., 2019). The emission profiles of other sources were derived from the latest version of SPECIATE 5.1 database (US EPA, 2021). Table S1 and S2 respectively show the I/SVOCs-G-to-VOCs and I/SVOCs-P-to-POA ratios and their emission profiles for specific sources. The base emissions of anthropogenic VOCs (AVOCs) and POA (See Table S3) were taken from a high-resolution emission inventory for the year of 2017 developed in our previous study (An et al., 2021). The I/SVOCs emissions for each source category were allocated into 4 km × 4 km grids using the same method as the criteria pollutants.

2.2 Model configuration

We used Community Modeling and Analysis System (CMAQ version 5.3.2) to simulate the concentrations of air pollutants. The domain of the simulation is presented in Figure 1. The simulations were conducted for three nested grids with horizontal resolution of 36 km (D1), 12 km (D2) and 4 km (D3), respectively. D1 covers most of China and the surrounding countries including Japan and South Korea; D2 covers eastern China and D3 covers the entire YRD region and its surrounding land and waters.

https://doi.org/10.5194/acp-2022-268
Preprint. Discussion started: 28 April 2022


Atmospheric Chemistry and Physics Discussions

Meteorological fields were provided by the Weather Research and Forecasting (WRF version 3.7) model with 27 vertical layers extending to the tropopause (100 hpa). The initial and boundary conditions (ICs, BCs) in the WRF were based on the 1° × 1° reanalysis data from the National Centers for Environmental Prediction Final Analysis (NCEP-FNL). Physical options used in the WRF simulation are listed in Table S4.

The Sparse Matrix Operator Kernel Emissions (SMOKE, https://cmascenter.org/smoke) model was applied to process emissions for input to CMAQ. CMAQ version 5.3.2 (https://cmascenter.org/cmaq/) was used to simulate atmospheric pollutants concentrations. ICs and BCs of D1 domain are based on a Model For Ozone And Related Chemical Tracers (MOZART) global simulation (https://acom.ucar.edu/wrf-chem/mozart.shtml). For the inner D2 and D3 domain, ICs and BCs are extracted from the simulation results of the outer domains. Options selected for the CMAQ simulations include the SAPRC07 gas phase chemistry, the AERO7 aerosol scheme, the Regional Acid Deposition Model (RADM) model aqueous phase chemistry, ISORROPIA inorganic particulate thermodynamics.

The emission inventory developed in this study was used to produce the emission system in the YRD region while emissions beyond YRD were supplied by Multiresolution Emission Inventory for China (MEIC-2017, http://meicmodel.org), Shipping Emission Inventory Model (SEIM) (Liu et al., 2016), and the Model Inter-Comparison Study (MIX) emission inventory for 2010 (Li et al., 2017). The I/SVOC emission inventory outside the YRD region was developed by multiplying the VOCs and POA emissions with the average I/SVOCs-G-to-VOCs and I/SVOCs-P-to-POA ratios of major source categories like industry, vehicle, marine vessel, and residential.

https://doi.org/10.5194/acp-2022-268
Preprint. Discussion started: 28 April 2022

Atmospheric Chemistry and Physics Discussions

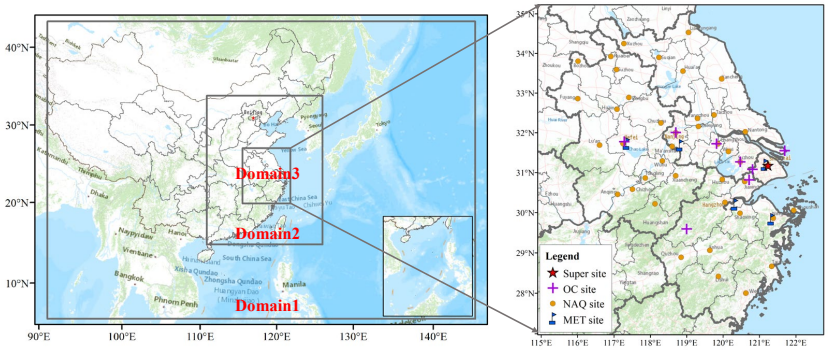

Figure 1. Modeling domain and locations of observation sites. The blue marks are meteorological monitoring sites. The yellow dots represent the national air quality monitoring sites. The purple crosses are the observation sites with $PM_{2.5}$ chemical composition measurements. The red star represents the observation site of AMS measurement.

SOA formed from I/SVOCs was estimated using the parameterization within the VBS framework in Lu et al. (2020). Specifically, the I/SVOC surrogates react with OH, generating four oxygenated organic species with volatility spanning from $C^* = 10^{-1}$ to 10^2 $\mu g \cdot m^{-3}$, which may exist in both gas and condensed phase. The rate coefficient (i.e., k_{OH}) and product yields (i.e., α_i, i=1, 2, 3, 4) for each primary I/SVOC species were derived based on previous laboratory results (Zhao et al., 2015; Zhao et al., 2016b). Multi-generation oxidation was considered by implementing further oxidation of the vapors from the initial oxidation, which redistributes the mass across the volatility bins of $C^* = 10^{-2}$ to 10^2 $\mu g \cdot m^{-3}$, and thus fragmentation and functionalization were included. Additionally, SOA formation from SVOCs were treated similarly, and more details can be found in Murphy et al. (2017).

2.3 Model simulations

To investigate the model performance on OA simulations and the contributions of different sources, we set 14 simulation cases using brute-force method (Zhang et al., 2005). Table 1 shows the settings for these 14 cases. First was BASE simulation case, in which the I/SVOC emissions was not included and the POA emissions were treated

https://doi.org/10.5194/acp-2022-268
Preprint. Discussion started: 28 April 2022

Atmospheric Chemistry and Physics Discussions

as non-volatile. The second was the IMPROVE case, which augmented the high-resolution I/SVOC emission inventory established in this study. In addition, the POA emissions in the IMPROVE simulation were split into both non-volatile and semivolatile parts. The non-volatile emissions were obtained by subtracting the I/SVOCs-P from the total POA. The semivolatile emissions, that was I/SVOCs-P emissions, were treated with variable gas–particle partitioning and multigenerational aging in this simulation case. We then used the difference between IMPROVE and BASE cases to evaluate the OA contributions from I/SVOC emissions. CASE1 to CASE12 respectively excluded the VOC and I/SVOC emissions from different sources. We used the differences between IMPROVE and CASE1−12 to quantify the contribution of each source to OA concentration.

Table 1. Settings of simulation cases.

Name	Emission settings	Notes
BASE	with VOC emissions, without I/SVOC emissions	base case
IMPROVE	with both VOC and I/SVOC emissions	to quantify the contributions of VOC and I/SVOC emissions to OA by comparing with BASE case
CASE1	only without industrial process VOC and I/SVOC emissions in the region	to quantify the contributions of VOC and I/SVOC emissions from different source categories to OA by comparing with IMPROVE case
CASE2	only without industrial solvent-use VOC and I/SVOC emissions in the region	
CASE3	only without mobile VOC and I/SVOC emissions in the region	
CASE4	only without residential VOC and I/SVOC emissions in the region	
CASE5	only without biomass burning VOC and I/SVOC emissions in the region	
CASE6	only without biogenic VOC emissions in the region	
CASE7	without VOC and I/SVOC emissions in the region	
CASE8	only without gasoline vehicle VOC and I/SVOC emissions in the region	
CASE9	only without diesel vehicle VOC and I/SVOC emissions in the region	
CASE10	only without diesel machinery VOC and I/SVOC emissions in the region	
CASE11	only without marine vessel VOC and I/SVOC emissions in the region	
CASE12	only without cooking VOC and I/SVOC emissions in the region	

2.4 Model evaluation

To capture the characteristics of OA with different meteorological features in the

https://doi.org/10.5194/acp-2022-268
Preprint. Discussion started: 28 April 2022


Atmospheric Chemistry and Physics Discussions

YRD region, we selected four periods to represent spring (Mar. 15th to Apr. 15th, 2019), summer (Jul. 1st to 31st, 2019), autumn (Oct. 15th to Nov. 15th, 2018), and winter (Dec. 1st to 31st, 2018) to conduct the simulations. Evaluations on model performance were made by comparing the simulation results with the observations obtained in the region, including 5 meteorological observation sites, 10 $PM_{2.5}$ chemical composition sites, and 41 national air quality monitoring sites, one in each city. The locations of the meteorological and air pollutant observation sites are shown in Figure 1.

We also used the observation data of an AMS and a GC-MS/FID system at the supersite in Shanghai to further verify the model performance on the simulation of POA, SOA, and key VOC precursors. Details of AMS measurements and PMF analysis are provided in our previous study (Huang et al., 2021). A total of 55 PAMS (Photochemical Assessment Monitoring Stations) species were identified by the GC-MS/FID system including 27 alkanes, 11 alkenes, acetylene and 16 aromatics. The supersite was located on the top-floor of an eight-story building in Shanghai Academy of Environmental Sciences (SAES, 31°10' N, 121°25'E), 30 m above the ground. The site was in a typical residential and commercial area with significant influence from traffic emission. Several petrochemical and chemical industrial factories sit around 50 km away from the site to the south and southwest.

Model performance in simulation of meteorological parameters and major criteria air pollutants are summarized in Table S5 and S6. The mean bias (MB), mean gross error (MGE), root-mean-square error (RMSE), and index of agreement (IOA) of temperature, humidity, wind speed, and wind direction in each season are within the criteria recommended by Emery et al. (2001). Although the temperature in summer and winter, and wind speed in autumn and winter were slightly overestimated, their MGE and IOA values are within the uncertainties as recommended in Emery et al. (2001).

For the simulation of major criteria air pollutants, both mean fractional bias (MFB) and mean fractional error (MFE) of all pollutants met the criteria recommended by Boylan and Russell (2006). Since the addition of I/SVOC emissions would change the

https://doi.org/10.5194/acp-2022-268
Preprint. Discussion started: 28 April 2022


Atmospheric Chemistry and Physics Discussions

$PM_{2.5}$ simulation results, we thus presented the statistical results for both BASE and IMPROVE cases in the Table S6. The modeled SO_2 was slightly overestimated, which is likely due to the faster than expected reduction of SO_2 emissions, resulting in overestimation of SO_2 emissions in the emission inventory. On the contrast, the modeled NO_2 were underestimated in spring, autumn, and winter, likely due to the overestimation of wind speed in these seasons. The modeled O_3 and $PM_{2.5}$ were slightly overestimated in the IMPROVE simulation case. Overall, the simulated meteorological parameters and major criteria air pollutants are consistent with the observations.

3. Results and discussion

3.1 I/SVOC emission inventory

3.1.1 Source-specific I/SVOC emissions

Table 2 shows the I/SVOC emission inventories in gas- and particle-phase for detailed source category for year 2017 in the YRD region. The total I/SVOC-G emission in the YRD region was 1128.26 Gg in 2017, lower than that in Wu et al. (2021) of 136 Gg, but higher than the estimate in Huang et al. (2021b) of 73 Gg. The I/SVOC emissions in both Wu et al. (2021) and Huang et al. (2021b) were estimated by the POA scaling factor method. However, I/SVOCs-G emissions usually have stronger correlation with AVOCs, which is fully in gas-phase, other than POA in particle-phase (Lu et al., 2018). Especially for the industrial sectors, where gaseous organics dominate the primary organic emissions, there must be considerable uncertainties if POA scaling factor method is used for the estimation of I/SVOCs-G emissions.

We found industrial solvent-use was the largest contributor (489.38 Gg, 43.38%) of total S/IVOCs-G emissions, followed by industrial process sources (249.35 Gg, 22.10%), mobile source (320.40 Gg, 28.40%), residential source (58.57 Gg, 5.19%), and agriculture source (10.56 Gg, 0.94%). Specifically, chemical production, textile, and solvent-based coating were major sectors of I/SVOCs-G emissions in the YRD region, accounting for 21.59%, 20.37%, and 15.33% of the total I/SVOCs-G emission,

https://doi.org/10.5194/acp-2022-268
Preprint. Discussion started: 28 April 2022


Atmospheric Chemistry and Physics Discussions

and their contributions to AVOC emissions were 20.70%, 2.22%, and 23.42%, respectively (See Table S3). It is interesting to note that the I/SVOCs-to-VOCs ratios are largely different for different sources. For example, the textile industry only accounted for 2.22% of the total AVOC emissions in the YRD region but contributed to 20.37% of the I/SVOC-G emissions due to its higher I/SVOCs-to-VOCs ratio (2.473). Another example is water-based coatings, whose VOC emissions were approximately 10.2% of solvent-based coatings, while their I/SVOC emissions were 29.1% of those from solvent-based coatings. These findings indicate that reductions in VOC emissions not necessarily corresponds to the simultaneous reductions in I/SVOCs emissions and subsequent SOA formation, which should be considered in future control strategies. (Yuan et al., 2010).

For I/SVOCs-G emission of mobile origin, the major contributors were gasoline vehicle, diesel vehicle, and non-road diesel machinery, accounting for 13.52%, 10.59%, and 3.96%, respectively. The total I/SVOCs-G emissions from gasoline and diesel vehicles were 272.03 Gg, much higher than the results reported in Liu et al. (2017) (29.58 Gg) and Huang et al. (2021b) (16.0 Gg) using the emission factor method, which likely underestimates the emission factors of I/SVOCs due to the lack of localized emission factors. Our tunnel experiment results show that the average IVOCs emission factors of gasoline and diesel vehicles were 15.3 $mg \cdot km^{-1}$ and 219.8 $mg \cdot km^{-1}$ (Tang et al., 2021), which were significantly higher than those used in the above studies (Liu et al., 2017; Huang et al., 2021b). More comprehensive localized emission measurements are advocated to better constrain the I/SVOC emissions from mobile sources.

I/SVOCs-P emissions were 118.39 Gg, occupying 58.70% of the POA emissions in the region. POA emissions and contributions from different sources can be found in Table S3. The largest contributor of I/SVOCs-P emissions came from biomass burning and diesel vehicle, accounting for 58.08% and 20.53% of the total, followed by gasoline vehicle (7.12%), biomass burning (6.08%), diesel machinery (4.14%), and marine vessel (4.05%).

https://doi.org/10.5194/acp-2022-268
Preprint. Discussion started: 28 April 2022

Atmospheric Chemistry and Physics Discussions

335 **Table 2.** Source-specific emissions of I/SVOCs for the year 2017 in the YRD region.

Source		I/SVOCs-G		I/SVOCs-P	
		Gg	%	Gg	%
Industrial process	Oil refinery	5.63	0.50		
	Chemical production	243.60	21.59		
	Pulp and paper	0.11	0.01		
Industrial solvent-use	Textile	229.78	20.37		
	Leather tanning	3.83	0.34		
	Timber processing	31.08	2.76		
	Furniture coating	1.32	0.12		
	Solvent-based coating	173.02	15.33		
	Water-based coating	50.32	4.46		
	Dry cleaning	0.02	0.00		
	Paint remover	0.01	0.00		
Mobile source	Gasoline vehicle	152.58	13.52	8.44	7.12
	Diesel vehicle	119.45	10.59	24.31	20.53
	Fuel evaporation	0.69	0.06		
	Diesel machinery	44.72	3.96	4.90	4.14
	Marine vessel	2.33	0.21	4.79	4.05
	Aircraft	0.64	0.06		
Residential source	Coal combustion	2.73	0.24		
	Residential solvent-use	35.29	3.13		
	Cooking	20.55	1.82	68.76	58.08
Agriculture source	Biomass burning	10.56	0.94	7.19	6.08
Total		1128.26	100.00	118.39	100.00

336 3.1.2 Volatility distributions of I/SVOCs

337 With the I/SVOC emission profiles of each source category (Table S1 and S2), we
338 successfully compiled the volatility distribution of I/SVOC emissions from different
339 sources as well as their gas-particle distribution (Figure 2). The I/SVOC emissions
340 generally showed an increasing trend with the increase of volatility. As shown in Figure
341 2(a), IVOC emissions (logC* bins at 3−6) accounted for 89% of the total I/SVOCs
342 emissions, overwhelmingly dominated by industrial process and mobile sources.
343 SVOCs (logC* bins at 0−2) and low-volatile organic compounds (LVOCs, logC* bins
344 at -1) contributed to 10% and 1% of the total I/SVOCs emissions. In terms of the
345 contributing sectors, mobile sources, industrial process, and solvent-use dominated the

https://doi.org/10.5194/acp-2022-268
Preprint. Discussion started: 28 April 2022


Atmospheric Chemistry and Physics Discussions

346 total I/SVOC emissions. While the IVOCs were equally contributed by above-listed
347 three sources, industrial process and mobile sources dominated the SVOCs and LVOCs
348 emissions.

349 We further investigated the contributions of different volatility bins to each source
350 category. The mobile source was dominated by IVOC emission (88%). Note that we
351 also split the aromatic IVOCs emission from mobile source using the method in Lu et
352 al. (2020) and found that aromatic IVOCs accounted for 23% of the total I/SVOC
353 emissions from the mobile source. The industrial process and solvent-use sources were
354 also dominated by IVOC emissions, accounting for 81% and 97%, respectively. The
355 volatility distribution of residential sources was relatively uniform, with IVOCs,
356 SVOCs and LVOCs accounting for 46%, 27% and 27%. Agricultural (i.e., biomass
357 burning) sources were more concentrated in IVOCs, accounting for 71%, while SVOCs
358 and LVOCs accounted for 20% and 9%, respectively. Except agricultural sources,
359 I/SVOC emissions from all sources are dominated by gas-phase species. The
360 agricultural sources were dominated by particle-phase species, taking up 78% of the
361 total I/SVOC emissions with the VBS bins concentrated in the logC* range of 0−4. It
362 should be noted that other than mobile sources, the emission profiles of the other
363 sources were mainly derived from SPECIATE 5.1 database (US EPA, 2021) in this
364 study, which may be inconsistent with real-world emissions in China. To further reduce
365 the uncertainty in this newly establish I/SVOC estimation inventory, measurements of
366 I/SVOC emissions from different local sources are therefore important and urgently
367 needed in the future.

https://doi.org/10.5194/acp-2022-268
Preprint. Discussion started: 28 April 2022

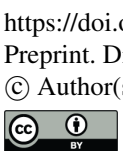

Atmospheric Chemistry and Physics Discussions

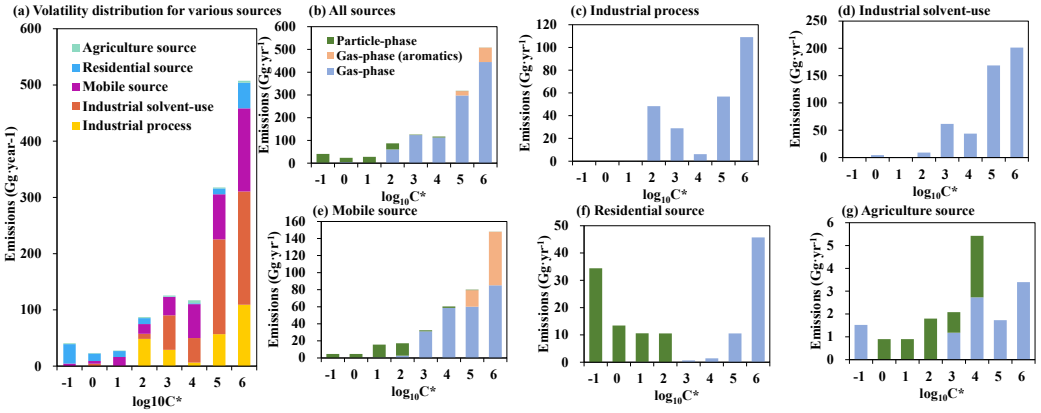

Figure 2. Volatility distributions of I/SVOCs emitted from different sources in the YRD region.

3.1.3 Spatial distributions of I/SVOC emissions in YRD region

Figure 3 shows the spatial distributions of source-specific I/SVOC emissions in the YRD region. The I/SVOC emissions were largely concentrated in city clusters in eastern YRD, and hotspots can also be observed in the northern urban agglomerations. The spatial distribution of total I/SVOC emissions was resulted from combined emissions from mobile, industrial process and solvent-use sources. The emissions from mobile and residential sources clustered into multiple hotspots in urban areas, while emissions from agricultural sources were mainly distributed in northern YRD, where frequent agricultural activities exist. The distribution of I/SVOC emissions was generally consistent with that of the VOC emissions in the eastern and central area of the region. But higher I/SVOC emissions than VOC emissions were observed in northern YRD (See Figure S1). This can be explained by the difference in I/SVOCs-G-to-VOCs ratios among different sources. For example, industrial and mobile sectors are major sources of I/SVOC emissions, yet AVOC emissions were mainly dominated by industrial sectors.

We also compare the spatial distributions of I/SVOC emissions with those of POA and BVOCs. We found that POA emissions were more concentrated in urban centers associated with mobile and residential sources (See Figure S1). BVOC emissions in the YRD region were mainly distributed in the southern area, where AVOC and IVOC

https://doi.org/10.5194/acp-2022-268
Preprint. Discussion started: 28 April 2022

Atmospheric Chemistry and Physics Discussions

emissions were relatively low. The difference in the spatial distributions of I/SVOC, AVOC, BVOC, and POA emissions implies that the sources of organic components in different areas of the region are quite different, which will be discussed in the following sections.

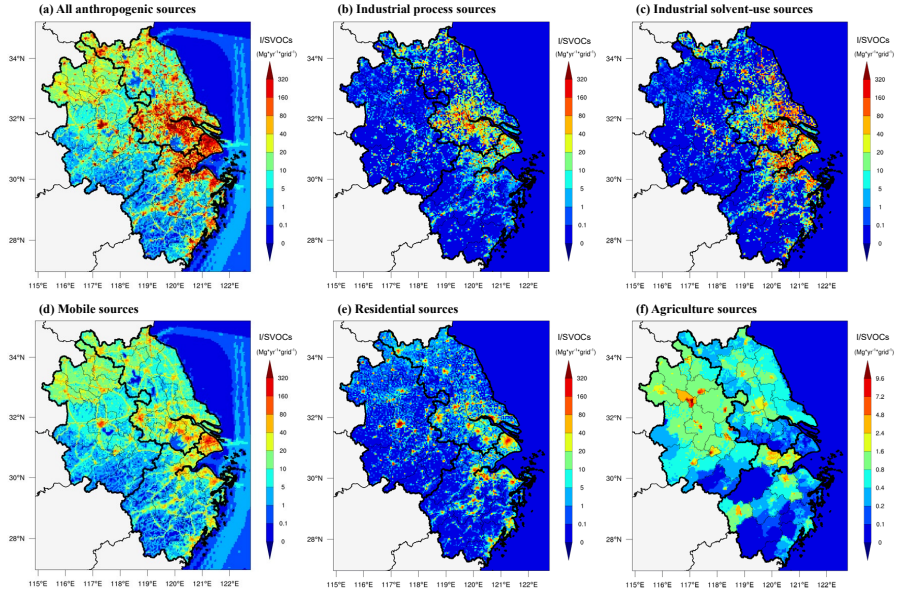

Figure 3. Spatial distributions of I/SVOC emissions from different source categories in the YRD region for the year 2017.

3.2 Comparison between model simulation and observation

3.2.1 Simulation results of VOCs and IVOCs

Since model performance on the simulation of VOCs are critical for SOA estimation, we first compare the modeled concentrations of VOCs with those of the measured at the SAES supersite for several aromatic VOCs, including benzene, toluene, and m-/p-/o-xylenes. As shown in Figure S2, the model simulation was able to capture the hourly variations of these species measured, with Pearson correlation coefficients (r) of 0.54−0.65, 0.45−0.60, 0.54−0.69 for toluene, xylene, and benzene respectively. Although the simulation results of toluene were 28% lower and xylene and benzene were 41% and 22% higher than those of the measured, the model results are within the uncertainties. Overall, the simulation results of the VOC species showed good

https://doi.org/10.5194/acp-2022-268
Preprint. Discussion started: 28 April 2022


Atmospheric Chemistry and Physics Discussions

agreements with the observations, which could be further used for the model simulation of SOA formation.

Long-term continuous observations of I/SVOC concentrations were sparse, so the simulation results of IVOCs were compared with those obtained from offline measurements reported in our previous studies (Li et al., 2019; Ren et al., 2020). The reported IVOC concentrations (sum of gas- and particle-phase concentrations) in summer and winter Shanghai in 2018 respectively varied between 1.5−17.2 and 2.2−43.1 $\mu g \cdot m^{-3}$ with average concentrations of 6.8 ± 3.7 and 18.2 ± 11.0 $\mu g \cdot m^{3}$. In this study, our modeled average concentrations of IVOCs in spring, summer, autumn, and winter at the SAES supersite in Shanghai were 12.8 ± 5.6, 9.0 ± 3.2, 12.2 ± 5.2, and 12.4 ± 7.6 $\mu g \cdot m^{-3}$, respectively. Although there was still a deviation of 20%−30% between the simulation and observation, not to mention the diurnal patterns and spatial distributions also remained unknown, the simulation results are at least comparable to those of the measured concentrations, suggesting the modeled I/SVOCs is appropriate to be used in the estimation of SOA production from different sources. Continuous long-term measurements of I/SVOC at multiple locations are strongly recommended in the future to improve the model performance and reduce the uncertainties in SOA estimation.

3.2.1 Simulation results of OA concentrations

Figure 4 presents the OA concentrations originated from different sources, including POA and SOA formed from AVOCs, BVOCs, and I/SVOCs, in four seasons in YRD from both BASE and IMPROVE simulations. Here we used the average of the modeled concentrations at 41 national air quality monitoring sites (See the yellow dots in Figure 1) to represent the regional average. The regional average concentration of OA (9.62 $\mu g \cdot m^{-3}$) in the IMPROVE simulation was 38% higher than that from BASE simulation (6.98 $\mu g \cdot m^{-3}$) due to the involvement of I/SVOCs in the IMPROVE simulation.

The seasonal average concentration of POA was 5.0 $\mu g \cdot m^{-3}$ in the BASE case, with

https://doi.org/10.5194/acp-2022-268
Preprint. Discussion started: 28 April 2022


Atmospheric Chemistry and Physics Discussions

435 the lowest in summer (3.3 μg m^{-3}) and the highest in winter (5.9 μg m^{-3}). High POA
436 concentrations in winter was mainly induced by the stagnant meteorological conditions
437 such as low wind speed and boundary layer height, and vice versa in summer. For the
438 spatial distributions as presented in Figure 5, POA concentrations in northern YRD were
439 high and mainly concentrated in urban areas, which was consistent with the
440 distributions of POA emissions (Figure S1). The POA concentrations in the IMPROVE
441 simulation were -3%−13% apart from those in the BASE simulation. In the IMPROVE
442 simulation, the POA was treated as semi-volatile, where gas–particle partitioning and
443 multigeneration oxidation were considered (Murphy et al., 2017). The differences
444 between these two cases were then determined by the competitive effects of
445 functionalization and fragmentation. In summer, more aged products were transferred
446 to higher-volatility bins to produce SOA and thus reduced POA concentrations.
447 BASE and IMPROVE simulations show similar results in the average
448 concentrations of SOA formed from AVOCs (AVSOA). The seasonal average
449 concentration of AVSOA was only 0.25 μg·m^{-3}, exhibiting very limited contribution to
450 the regional OA concentration, whereas average concentration of BVOC derived SOA
451 (BVSOA, 1.7 μg m^{-3}) was much higher than expected. Also, evident seasonal variations
452 were observed for BVSOA, with the highest in summer (2.48 μg·m^{-3}), followed by
453 spring (1.80 μg·m^{-3}), autumn (1.36 μg·m^{-3}), and winter (1.19 μg·m^{-3}). Hotspots of
454 BVSOA concentrations were concentrated in the western and southern YRD. The
455 observed seasonal variations and spatial distributions of BVOC derived SOA were
456 consistent with those of the BVOC emissions in YRD (Liu et al., 2018).
457 The average concentration of I/SVOC derived SOA (I/SVSOA) in IMPROVE
458 simulation was 2.26 μg·m^{-3}, with the highest in spring (2.73 μg·m^{-3}) and the lowest in
459 summer (1.87 μg·m^{-3}), which is a combined effect of emission, oxidation and
460 meteorological conditions. For example, Qin et al. (2022) suggested that in spring the
461 enhanced solar radiation and OH oxidation potentially promote the secondary
462 conversion from I/SVOCs to SOA. The low concentration in summer was likely due to

https://doi.org/10.5194/acp-2022-268
Preprint. Discussion started: 28 April 2022

Atmospheric Chemistry and Physics Discussions

463 the better meteorological conditions than the other seasons. By incorporating I/SVOC
464 emissions into the IMPROVE simulation, the modeled average SOA concentration in
465 the region increased from 1.96 (BASE) to 4.22 $\mu g \cdot m^{-3}$; and high concentrations of
466 I/SVSOA were observed in central and northern YRD. Overall, the addition of high-
467 resolution I/SVOC emissions significantly increase the SOA concentration by 116%,
468 which will be further constrained by the observation in next section.

469 To validate the model performance on regional OA simulation, we compared it
470 with the measured concentrations of organic carbon (OC) in $PM_{2.5}$ at multiple sites in
471 the YRD region (Figure S3). Although both BASE and IMPROVE simulations showed
472 good correlations with the observation as shown in Figures 6c, 6f, 6i, and 6l, OC
473 concentrations in IMPROVE simulations in different seasons were all higher than those
474 in the BASE simulations. In the BASE simulation, the modeled OC concentrations of
475 each season only explained 49% to 59% of the observations. With the addition of
476 I/SVOC emissions into IMPROVE simulation, the modeled OC concentrations much
477 better agreed with the observations, with modeled OC increased to 75% to 93% of the
478 observations. Details for the statistical evaluation of model performance on OC in
479 BASE and IMPROVE simulations are shown in Table S6.

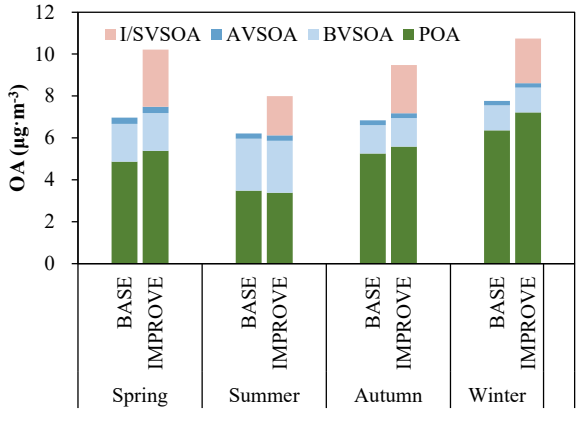

480

481 **Figure 4.** Comparisons of the regional average concentrations of POA and SOA formed from
482 AVOCs, BVOCs, and I/SVOCs in different seasons from the BASE and IMPROVE simulations.

https://doi.org/10.5194/acp-2022-268
Preprint. Discussion started: 28 April 2022

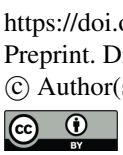

Atmospheric Chemistry and Physics Discussions

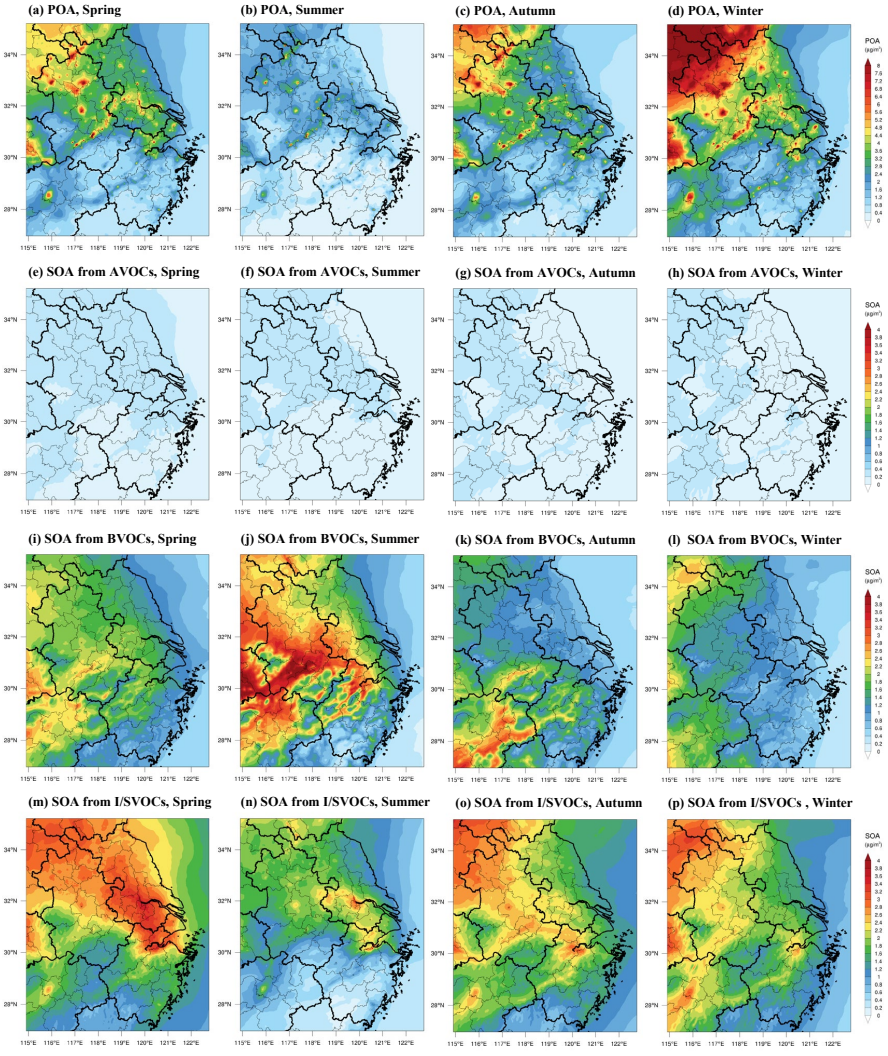

Figure 5. Spatial distributions of modeled POA and SOA formed from AVOCs, BVOCs, and I/SVOCs in different seasons in the IMPROVE simulation.

3.2.2 Temporal variations of OA components: simulation vs. AMS observation

To further validate the model performance on the simulations of POA and SOA, we compared the simulation results with those measured by an AMS at the SAES supersite. Both simulation and observation results were obtained for PM_1 aerosol particles (aerodynamic diameter < 1 μm). Figure 6 shows that the simulation results of POA, SOA and OA were similar to the observation results not only in average

https://doi.org/10.5194/acp-2022-268
Preprint. Discussion started: 28 April 2022


Atmospheric Chemistry and Physics Discussions

492 concentration levels but also in temporal variations. For POA, the BASE and
493 IMPROVE simulations agree with each other (Figure S4) and both can reproduce the
494 observed concentrations and diurnal variations of POA though a small deviation of
495 3%−26% between the simulated and observed concentrations in different seasons still
496 existed. Similar to the observation results, the simulated POA concentrations peaked at
497 noon and early evening, which were mainly contributed by cooking emissions as
498 reported in our previous study (Huang et al., 2021).
499 For SOA, the average concentrations in spring, summer, autumn, and winter in
500 BASE simulation were 1.4, 1.6, 0.8, and 0.7 $\mu g \cdot m^{-3}$, respectively, which were only
501 13%−31% of those observed by the AMS (see Figure S4). The SOA simulation was
502 greatly improved in IMPROVE simulation with the modeled SOA concentrations of
503 4.2, 3.8, 2.7, and 2.4 $\mu g \cdot m^{-3}$ in spring, summer, autumn, and winter respectively. The
504 SOA concentrations in IMPROVE simulation were 1.4−2.4 times higher than those in
505 BASE simulation, which is 43% to 75% of the observation, indicating the large
506 contributions of I/SVOCs emissions to SOA production. The IMPROVE simulation
507 also demonstrated improvements in reproducing the temporal variations of SOA,
508 especially during the daytime (Figure 6e - 6h). Compared with the BASE simulation,
509 evident increases in SOA concentrations during daytime can be observed in IMPROVE
510 simulation, which agrees better with the observation, likely driven by photochemistry.
511 Although the SOA simulations were improved in all four seasons, best simulation
512 results were found in summer, when both the concentrations and diurnal variations of
513 SOA were well reproduced.
514 While our current results presented great improvements in SOA simulation, gaps
515 were still left between the simulation and observation especially during the nighttime.
516 The main reasons for the discrepancy between the simulated and measured SOA are:
517 (1) I/SVOC emissions from outside of the YRD region might be underestimated due to
518 the lack of detailed base emission inventory, resulting in the corresponding
519 underestimation of the transported SOA, which were prominent especially in autumn,

https://doi.org/10.5194/acp-2022-268
Preprint. Discussion started: 28 April 2022

Atmospheric Chemistry and Physics Discussions

winter and spring in Shanghai; (2) current model simulation only consider the oxidation processes driven by OH oxidation. However, an increasing body of experimental and observational evidence suggest that heterogeneous and multiphase reactions also played important roles in SOA formation especially during pollution episodes (Guo et al., 2020; Kim et al., 2021). Recent studies also found that nocturnal NO_3 oxidation was also an important route for SOA formation (Yu et al., 2019; Decker et al., 2021). Yet mechanism and parameterizations of these processes remain unclear, making the involvement of these processes in the model difficult.

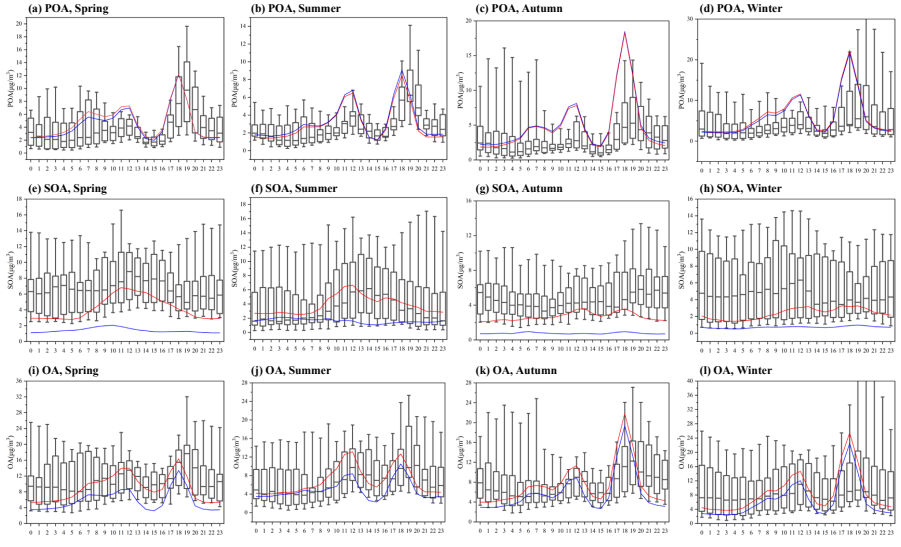

Figure 6. Diurnal patterns of modeled POA, SOA, and OA concentrations in different seasons and their comparisons with the observations at the SAES supersite. The boxplots represent the diurnal patterns of the AMS observations. The blue and red lines respectively represent the diurnal patterns of the simulation results in BASE and IMPROVE cases.

3.3 OA source contributions

3.3.1 POA and SOA sources in the region

Based on the high-resolution I/SVOC emission inventory established in this study, we successfully simulated the POA and SOA concentrations from each source. Table 3 summarizes the regional average concentrations of POA and SOA originated from different sources and their relative contributions. Residential POA dominated the

https://doi.org/10.5194/acp-2022-268
Preprint. Discussion started: 28 April 2022


Atmospheric Chemistry and Physics Discussions

539 regional OA, with average concentrations ranged from 1.90 to 3.51 μg·m^{-3} in different
540 seasons, accounting for 23.79%–32.66% of the total OA, among which cooking
541 emission is the dominant source (*ca.* 94%) of residential POA. Other POA sources
542 include industrial, biomass burning, and mobile sources, accounting for 7.25%–8.67%,
543 4.94%–10.23%, and 3.42%–4.35% of the total OA, respectively. The cumulative
544 fraction of POA in total OA from industrial and mobile sources was 10.67%–12.86%,
545 close to that of HOA (15%) observed by the AMS measurement in Shanghai (Figure
546 S5).

547 Industrial sources were the main source of SOA in the YRD region, with average
548 SOA concentrations of 0.91–1.38 μg·m^{-3} in four seasons, accounting for 8.71%–13.65%
549 of the total OA, among which, industrial process and solvent-use sources had almost
550 equal contributions. Mobile sources were the second largest source of SOA in this
551 region, with an average concentration of 0.37–0.57 μg·m^{-3}, accounting for 3.42%–6.09%
552 of the total OA. Among them, the source contribution of gasoline vehicles to SOA was
553 1.80%–2.84%, and that of diesel vehicles was 1.20%–2.44%. BVSOA showed
554 significant seasonal differences with concentrations of 0.76, 1.61, 0.59, and 0.12 μg·m^{-3},
555 respectively in spring, summer, autumn, and winter, accounting for 7.40%, 20.20%,
556 6.21%, and 1.14% of the total OA.

557 Overall, cooking emission was the major source of POA in YRD, accounting for
558 27.69%–32.45% of the total OA, which is consistent with our observations in Shanghai
559 (Huang et al., 2021; Zhu et al., 2021). Both simulations and observations demonstrated
560 higher contributions of cooking emission in urban China than those reported overseas
561 (17%–18%) (Chen et al., 2021), which is attributed to the difference between Asian-
562 style and Western-style cooking. The results emphasize that cooking emission has
563 become a non-negligible source of non-fossil carbon in urban areas in eastern China.
564 Contributions from industrial sources were running the second among all sources,
565 accounting for 16.51%–21.64% of OA and 23.33%–28.57% of SOA, which is
566 attributed to the high I/SVOC emissions from industrial sources and is consistent with

https://doi.org/10.5194/acp-2022-268
Preprint. Discussion started: 28 April 2022

Atmospheric Chemistry and Physics Discussions

previous studies (Miao et al., 2021). Other sources mainly include mobile sources (7.77% to 9.68% of OA) and biomass burning (5.63%−11.15% of OA). Specifically, diesel and gasoline vehicles were the major contributors among mobile sources, with higher contribution from the former (3.98%−4.68%) than the latter (2.79%−3.73%), followed by diesel machinery (0.86%−1.06%) and marine vessels (0.15%−0.30%). The contribution of biomass burning was highest in winter (11.15%) compared to contributions of 5.63%−7.29% in other seasons and it was even higher than contribution of mobile sources (7.77%) in winter. The remaining 15.44%−27.03% of OA was from super region scale, which represented OA originated from emissions outside the YRD region.

Table 3. POA and SOA source contributions of different emission sources in each season in the YRD region.

Sources	Spring		Summer		Autumn		Winter	
	conc. ($\mu g \cdot m^{-3}$)	ratio (%)	conc. ($\mu g \cdot m^{-3}$)	ratio (%)	conc. ($\mu g \cdot m^{-3}$)	ratio (%)	conc. ($\mu g \cdot m^{-3}$)	ratio (%)
POA	5.38	52.71	3.39	42.40	5.59	58.86	7.21	67.11
Industrial sources	0.83	8.10	0.58	7.25	0.82	8.67	0.84	7.80
Industrial process	0.73	7.19	0.52	6.54	0.73	7.74	0.75	6.98
Industrial solvent-use	0.09	0.91	0.06	0.71	0.09	0.93	0.09	0.82
Mobile sources	0.42	4.11	0.27	3.42	0.40	4.19	0.47	4.35
Gasoline Vehicles	0.10	0.99	0.07	0.89	0.09	0.99	0.11	0.99
Diesel Vehicles	0.26	2.53	0.16	2.01	0.25	2.61	0.30	2.78
Diesel machinery	0.04	0.42	0.03	0.40	0.04	0.45	0.05	0.48
Marine vessel	0.02	0.17	0.01	0.13	0.01	0.14	0.01	0.10
Residential sources	2.63	25.75	1.90	23.79	2.93	30.88	3.51	32.66
Cooking	2.44	23.92	1.85	23.15	2.80	29.54	3.18	29.61
Other residential	0.19	1.82	0.05	0.64	0.13	1.34	0.33	3.05
Biomass burning	0.70	6.88	0.39	4.94	0.56	5.90	1.10	10.23
Super region	0.80	7.88	0.24	3.00	0.87	9.22	1.30	12.07
SOA	4.83	47.29	4.60	57.60	3.90	41.14	3.53	32.89
Industrial sources	1.38	13.54	1.09	13.65	0.91	9.56	0.94	8.71
Industrial process	0.71	6.94	0.53	6.58	0.51	5.38	0.54	4.99
Industrial solvent-use	0.67	6.61	0.57	7.08	0.40	4.18	0.40	3.71
Mobile sources	0.57	5.57	0.49	6.09	0.38	3.98	0.37	3.42
Gasoline Vehicles	0.28	2.70	0.23	2.84	0.18	1.88	0.19	1.80
Diesel Vehicles	0.22	2.15	0.20	2.44	0.15	1.56	0.13	1.20

https://doi.org/10.5194/acp-2022-268
Preprint. Discussion started: 28 April 2022


Atmospheric Chemistry and Physics Discussions

Diesel machinery	0.06	0.59	0.05	0.66	0.04	0.45	0.04	0.38
Marine vessel	0.01	0.13	0.01	0.14	0.01	0.09	0.01	0.05
Residential sources	0.39	3.78	0.36	4.54	0.26	2.78	0.31	2.84
Cooking	0.39	3.78	0.36	4.54	0.26	2.78	0.31	2.84
Other residential	0.00	0.00	0.00	0.00	0.00	0.00	0.00	0.00
Biomass burning	0.04	0.41	0.06	0.69	0.01	0.11	0.10	0.92
Biogenic	0.76	7.40	1.61	20.20	0.59	6.21	0.12	1.14
Super region	1.69	16.59	0.99	12.44	1.76	18.51	1.70	15.86

3.3.2 Spatial distributions of SOA originated from different sources

Figure 7 shows the spatial distributions of modeled SOA originated from different sources in each season in YRD region. Note that we only considered the SOA formed from the intraregional VOC and I/SVOC emissions, excluding those transported from the super region. A large spatial variability was observed for the sources of SOA driven by emissions. For example, industrial and mobile SOA concentrated in the eastern and central YRD, where I/SVOC emissions were high (Figure 3). Residential and agricultural SOA presented a more uniform spatial distribution than industrial and mobile SOA, with enhanced formation in central and western YRD (Figures 7i-7l).

Although absolute source-dependent SOA concentrations differ in different seasons, low spatial variabilities were observed for different seasons. Industrial, mobile, and residential sources were the predominant contributors to SOA formation in eastern and central YRD, especially for the area along the Hangzhou Bay and Yangtze River driven by the enhanced I/SVOC emissions. The spatial distributions of BVSOA have been discussed above and will not be detailed here.

https://doi.org/10.5194/acp-2022-268
Preprint. Discussion started: 28 April 2022

Atmospheric Chemistry and Physics Discussions

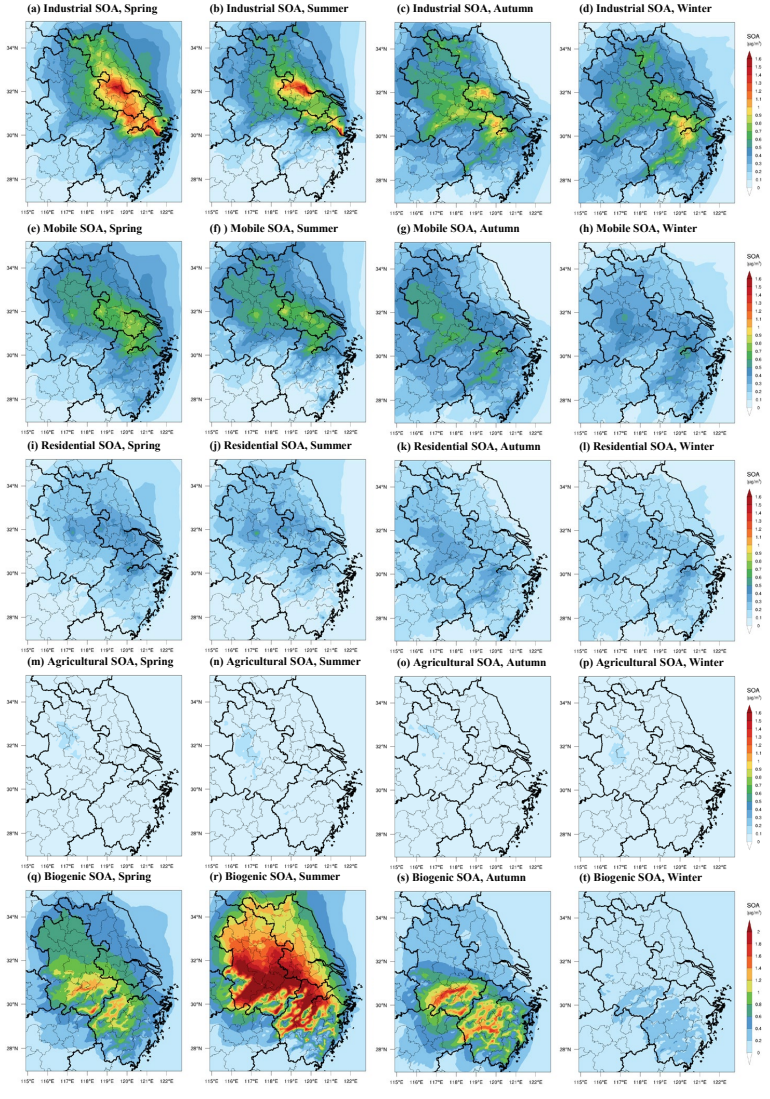

Figure 7. Spatial distributions of modeled SOA concentrations from different sources in each season in YRD region.

3.3.3 Predominant OA sources in sub-regions of YRD

To characterize the source contributions in different parts of the region, we categorized the simulation region into six sub-regions: northern YRD, western YRD, central YRD, eastern YRD and southern YRD. And six representative cities in theses six regions were further selected for detailed comparison in source contributions,

https://doi.org/10.5194/acp-2022-268
Preprint. Discussion started: 28 April 2022


Atmospheric Chemistry and Physics Discussions

including Xuzhou (XZ), Hefei (HF), Nanjing (NJ), Hangzhou (HZ), Shanghai (SH) and Jinhua (JH). Figure 8 shows their locations and OA source contributions during summer and winter.

In Northern YRD, represented by XZ, enhanced contribution from super-regional scale to the local OA was observed for both winter (53.2%) and summer (28.9%) and the contributions from industrial processes (23.4% in winter and 18% in summer) were also higher than other sub-regions. Other major sources include biogenic (12.6%) and cooking emissions (14.7%) in summer and cooking (9.3%) and other residential emissions (10.4%) in winter. Taken together, supe-regional transportation and industrial processes are predominant contributors of OA in northern YRD, accounting for 76.6% and 46.9% in summer and winter respectively, followed by cooking emissions.

In western YRD, represented by HF, cooking emission was the largest contributor to OA with contributions of 21.4% and 32.5% in both summer and winter respectively, followed by super-regional contributions of 17.4% (summer) and 25.8% (winter). Other major sources also include mobile source of 14%, biogenic source in summer (17.5%) and industrial processes in both summer (12.6%) and winter (10.5%). In central YRD, represented by NJ and HZ, the relative source contributions were very similar to those in western YRD, with predominant contributions from cooking (24.3%-38%), followed by super-regional transportation (8.8%-27.8%), industrial processes (10.9%-18.4%) and mobile source (10%-13%).

In eastern YRD, represented by SH, the largest OA source was cooking emission, account for 25.5% and 43.6% of OA in summer and winter respectively, followed by mobile sources of 16%, super-regional transportation of 13.4% (summer) and 25.8% (winter) and industrial processes of 19.4% (summer) and 10.5% (winter). In southern YRD, represented by JH, while biogenic contribution was prevailing in summer (37%), super-regional transportation was significant in winter (28.7%). Similar to other sub-regions, other major sources also included the contributions of cooking emission of 14.8% (summer) and 14.3% (winter), industrial processes of 8.7% (summer) and 17.4%

https://doi.org/10.5194/acp-2022-268
Preprint. Discussion started: 28 April 2022


Atmospheric Chemistry and Physics Discussions

(winter) and mobile sources of 13%. Yet southern YRD presented more evident increase in the contribution from industrial solvent-use compared with other sub-regions.

To summarize, cooking, super-regional transportation, industrial process and mobile sources were the predominant sources of OA in all sub-regions regardless of the season, albeit enhanced contributions from biogenic sources to the OA formation in summer was observed, especially in southern YRD. High contributions of cooking sources were in accordance with the distributions of populations and high contributions of mobile sources were somewhat expected, especially in the city centers. Source contributions of OA varies in the intraregional scale implies that more targeted control measures need to be designed according to the emission features of each city. Specifically, for densely populated area, it is necessary to strengthen the future control strategy of cooking emissions; special attention needs to be paid to the I/SVOC emissions from industrial sources in eastern, central, and northern YRD region; mobile sources show its significance in urban aera of the region, dominated by the equal contributions from gasoline and diesel vehicles, indicating further reductions on the I/SVOCs from vehicle emissions are therefore critical for pollution control on city scale.

https://doi.org/10.5194/acp-2022-268
Preprint. Discussion started: 28 April 2022

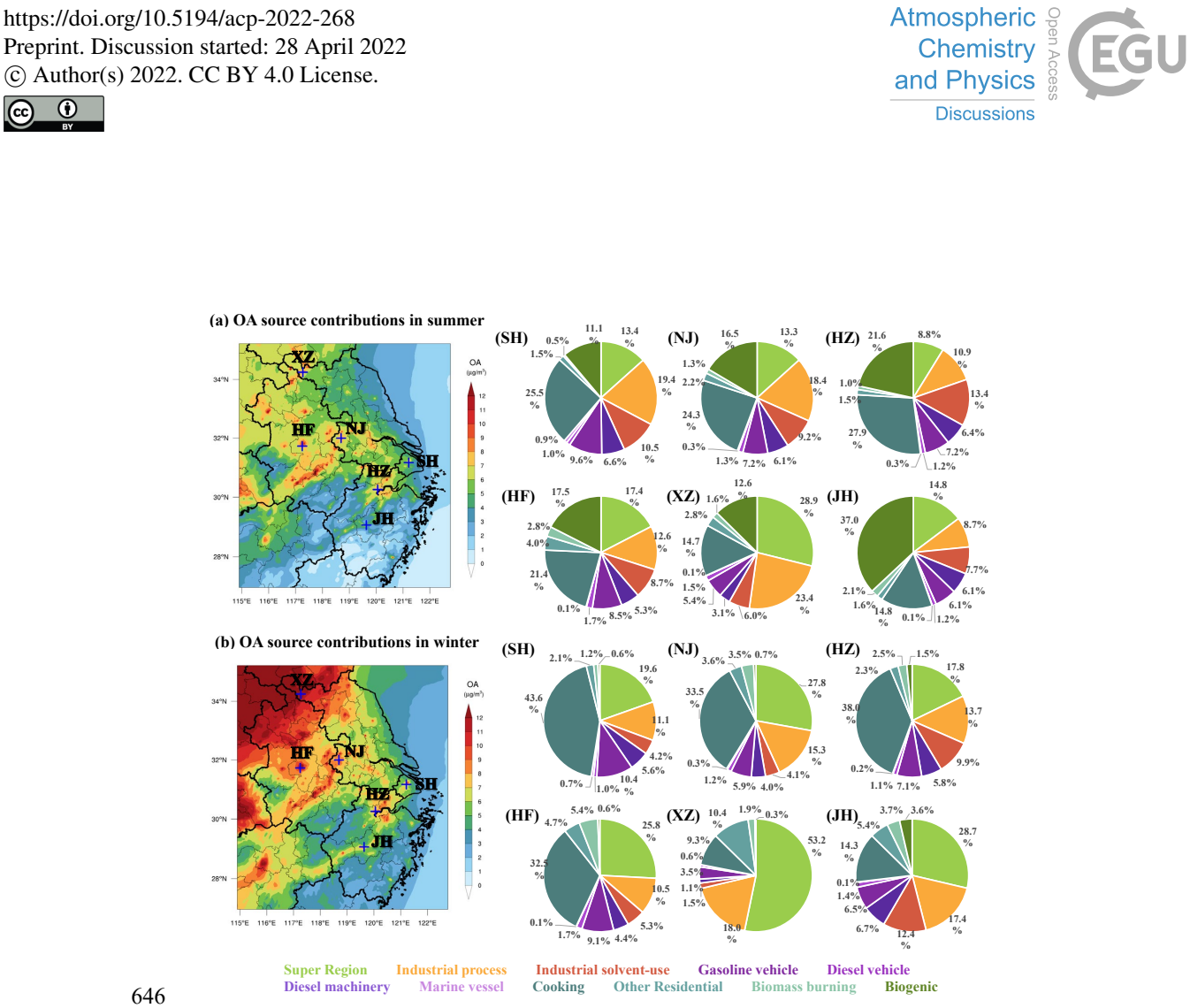

Figure 8. Source contributions of modeled OA concentrations from different sources during summer and winter in different cities of the region.

4. Conclusions

In this study, we established a high-resolution I/SVOC emission inventory with detailed source profiles and applied it into CMAQ v5.3 to simulate POA and SOA formation in YRD region of China. With the addition of I/SVOC emissions, simulation results show significant improvements on both temporal variations and spatial distributions of OA. Compared with the BASE simulation, where I/SVOC emissions were not included, the simulated SOA increased by 1.2 times in IMPROVE simulation, highlighting the significant contributions of I/SVOC emissions to SOA production. The remaining 20% underestimation of OA indicates that future work is still needed in bridging the gap between simulation and observations, such as, measuring local emission factors and source profiles of I/SVOC from various local sources, updating

https://doi.org/10.5194/acp-2022-268
Preprint. Discussion started: 28 April 2022


Atmospheric Chemistry and Physics Discussions

SOA formation mechanisms in model framework.

With the addition of source specific I/SVOC emissions, we successfully quantified the contribution of each source to POA and SOA concentrations in YRD. For POA, cooking emission is the predominant source, which concentrates in urban area of YRD in accordance with the population distribution. For SOA, for the first time, we demonstrate that I/SVOCs from industrial sources are dominant contributor, followed by those from mobile sources. In summer, the contributions of biogenic emission to total SOA are also non-negligible, especially for the cities in southern YRD. Spatial and seasonal variations in the source contributions suggest that control strategies for OA pollution should vary by cities and seasons. On regional scale, cooking emissions has been emerging as an important POA source, not to mention their impacts on SOA formation are not yet certain. Our results suggest the control measures on the cooking emissions should be strengthened in the future for the further reduction of POA. We also found that SOA in the region is primarily contributed by industrial I/SVOC emissions, which urges in-depth studies of emission factors and source profiles of I/SVOC emissions from industrial sources as well as the corresponding control measures. On intraregional scale, for urban area, continuous reduction in I/SVOC emissions from mobile sources, especially gasoline and diesel vehicles, are effective measures in the mitigation of urban air pollution, which is also technically feasible as has been demonstrated in Qi et al. (2021). Continuous improvement in emission standards is one way to promote the reduction of motor vehicle related SOA.

Data availability

The gridded emissions of I/SVOCs from various sources for the YRD region developed by this study at a horizontal resolution of 4 km × 4 km can be downloaded from the following website (https://doi.org/10.6084/m9.figshare.19536082.v1). Additional related data are available upon request by contacting the corresponding author (Cheng Huang; huangc@saes.sh.cn).

https://doi.org/10.5194/acp-2022-268
Preprint. Discussion started: 28 April 2022


Atmospheric Chemistry and Physics Discussions

Supplement

The supplement related to this article is available online.

Author contributions

CH, JA, DH, and MQ designed the research. CH and JA developed the I/SVOC emission inventory. JA, MQ, and RY performed the model. DH, LQ, MZ, YL, SZ, and QW collected the observation data. CH, JA, DH, and HW analyzed the results. CH, JA, and DH wrote the paper.

Competing interests

The authors declare that they have no conflict of interest.

Acknowledgement

We thank the supports from the National Natural Science Foundation of China, the Science and Technology Commission of the Shanghai Municipality, and the Shanghai Municipal Bureau of Ecology and Environment.

Financial support

This work has been supported by the National Natural Science Foundation of China (grant nos. 21777101), the Science and Technology Commission of the Shanghai Municipality (grant no. 21230711000), the Shanghai Municipal Bureau of Ecology and Environment Fund Project (grant no. 202001; 202114), and the State Environmental Protection Key Laboratory of Formation and Prevention of Urban Air Pollution Complex (grant no. CX2020080576).

References

An, J., Huang, Y., Huang, C., Wang, X., Yan, R., Wang, Q., Wang, H., Jing, S., Zhang, Y., Liu, Y., Chen, Y., Xu, C., Qiao, L., Zhou, M., Zhu, S., Hu, Q., Lu, J., and Chen, C.: Emission inventory of air pollutants and chemical speciation for specific anthropogenic sources based on local measurements in the Yangtze River Delta region, China, Atmos. Chem. Phys., 21, 2003–2025, 2021.

Boylan, J. W., and Russell, A. G.: PM and light extinction model performance metrics, goals,

https://doi.org/10.5194/acp-2022-268
Preprint. Discussion started: 28 April 2022


Atmospheric Chemistry and Physics Discussions

and criteria for three-dimensional air quality models, Atmos. Environ., 40, 4946–4959, 2006.

Cai, S., Zhu, L., Wang, S., Wisthaler, A., Li, Q., Jiang, J., and Hao, J.: Time-resolved intermediate-volatility and semivolatile organic compound emissions from household coal combustion in northern China, Environ. Sci. Technol., 53, 9269−9278, 2019.

Chen, W., Ye, Y., Hu, W., Zhou, H., Pan, T., Wang, Y., Song, W., Song, Q., Ye, C., Wang, C., Wang, B., Huang, S., Yuan, B., Zhu, M., Lian, X., Zhang, G., Bi, X., Jiang, F., Liu, J., Canonaco, F., Prevot, A. S. H., Shao, M., and Wang, X.: Real-time characterization of aerosol compositions, sources, and aging processes in Guangzhou during PRIDE-GBA 2018 campaign, J. Geophys. Res., Atmos., 126, e2021JD035114, 2021.

Crippa, M., Canonaco, F., Lanz, V. A., Äijälä, M., Allan, J. D., Carbone, S., Capes, G., Ceburnis, D., Dall'Osto, M., Day, D. A., DeCarlo, P. F., Ehn, M., Eriksson, A., Freney, E., Hildebrandt Ruiz, L., Hillamo, R., Jimenez, J. L., Junninen, H., Kiendler-Scharr, A., Kortelainen, A. M., Kulmala, M., Laaksonen, A., Mensah, A. A., Mohr, C., Nemitz, E., O'Dowd, C., Ovadnevaite, J., Pandis, S. N., Petäjä, T., Poulain, L., Saarikoski, S., Sellegri, K., Swietlicki, E., Tiitta, P., Worsnop, D. R., Baltensperger, U., and Prévôt, A. S. H.: Organic aerosol components derived from 25 AMS data sets across Europe using a consistent ME-2 based source apportionment approach, Atmos. Chem. Phys., 14, 6159–6176, 2014.

Cross, E. S., Hunter, J. F., Carrasquillo, A. J., Franklin, J. P., Herndon, S. C., Jayne, J. T., Worsnop, D. R., Miake-Lye, R. C., and Kroll, J. H.: Online measurements of the emissions of intermediate-volatility and semi-volatile organic compounds from aircraft, Atmos. Chem. Phys., 13, 7845–7858, 2013.

Decker, Z. C. J., Robinson, M. A., Barsanti, K. C., Bourgeois, I., Coggon, M. M., DiGangi, J. P., Diskin, G. S., Flocke, F. M., Franchin, A., Fredrickson, C. D., Gkatzelis, G. I., Hall, S. R., Halliday, H., Holmes, C. D., Gregory Huey, L., Lee, Y. R., Lindaas, J., Middlebrook, A. M., Montzka, D. D., Moore, R., Andrew Neuman, J., Nowak, J. B, Palm, B. B., Peischl, J., Piel, F., Rickly, P. S., Rollins, A. W., Ryerson, T. B., Schwantes, R. H., Sekimoto, K.,

https://doi.org/10.5194/acp-2022-268
Preprint. Discussion started: 28 April 2022


Atmospheric Chemistry and Physics Discussions

742 Thornhill, L., Thornton, J. A., Tyndall, G. S., Ullmann, K., Van Rooy, P., Veres, P. R.,
743 Warneke, C., Washenfelder, R. A., Weinheimer, A. J., Wiggins, E., Winstead, E., Wisthaler,
744 A., Womack, C., and Brown, S. S.: Nighttime and daytime dark oxidation chemistry in
745 wildfire plumes: an observation and model analysis of FIREX-AQ aircraft data, Atmos.
746 Chem. Phys., 21, 16293–16317, 2021.
747 Donahue, N. M., Robinson, A. L., and Pandis, S. N.: Atmospheric organic particulate matter:
748 From smoke to secondary organic aerosol, Atmos. Environ., 43, 94–106, 2009.
749 Donahue, N. M., Robinson, A. L., Stanier, C. O., and Pandis, S. N.: Coupled Partitioning,
750 Dilution, and Chemical Aging of Semivolatile Organics, Environ. Sci. Technol., 40, 2635–
751 2643, 2006.
752 Drozd, G. T., Weber, R. J., and Goldstein, A. H.: Highly resolved composition during diesel
753 evaporation with modeled ozone and secondary aerosol formation: Insights into pollutant
754 formation from evaporative intermediate volatility organic compound sources, Environ.
755 Sci. Technol., 55, 5742−5751, 2021.
756 Drozd, G. T., Zhao, Y., Saliba, G., Frodin, B., Maddox, C., Oliver Chang, M.-C., Maldonado,
757 H., Sardar, S., Weber, R. J., Robinson, A. L., and Goldstein, A. H.: Detailed speciation of
758 intermediate volatility and semivolatile organic compound emissions from gasoline
759 vehicles: Effects of cold-starts and implications for secondary organic aerosol formation,
760 Environ. Sci. Technol., 53, 1706–1714, 2019.
761 Emery, C., Tai, E., and Yarwood, G.: Enhanced meteorological modeling and performance
762 evaluation for two Texas ozone episodes, Prepared for the Texas natural resource
763 conservation commission, by ENVIRON International Corporation, 2001.
764 Gentner, D. R., Isaacman, G., Worton, D. R., Chan, A. W. H., Dallmann, T. R., Davis, L., Liu,
765 S., Day, D. A., Russell, L. M., Wilson, K. R., Weber, R., Guha, A., Harley, R. A., and
766 Goldstein, A. H.: Elucidating secondary organic aerosol from diesel and gasoline vehicles
767 through detailed characterization of organic carbon emissions, Proc. Natl. Acad. Sci., 109,
768 18318−18323, 2012.
769 Guo, J., Zhou, S., Cai, M., Zhao, J., Song, W., Zhao, W., Hu, W., Sun, Y., He, Y., Yang, C., Xu,

https://doi.org/10.5194/acp-2022-268
Preprint. Discussion started: 28 April 2022


Atmospheric Chemistry and Physics Discussions

X., Zhang, Z., Cheng, P., Fan, Q., Hang, J., Fan, S., Wang, X., and Wang, X.: Characterization of submicron particles by time-of-flight aerosol chemical speciation monitor (ToF-ACSM) during wintertime: aerosol composition, sources, and chemical processes in Guangzhou, China, Atmos. Chem. Phys., 20, 7595–7615, 2020.

Hallquist, M., Wenger, J. C., Baltensperger, U., Rudich, Y., Simpson, D., Claeys, M., Dommen, J., Donahue, N. M., George, C., Goldstein, A. H., Hamilton, J. F., Herrmann, H., Hoffmann, T., Iinuma, Y., Jang, M., Jenkin, M. E., Jimenez, J. L., Kiendler-Scharr, A., Maenhaut, W., McFiggans, G., Mentel, Th. F., Monod, A., Prévôt, A. S. H., Seinfeld, J. H., Surratt, J. D., Szmigielski, R., and Wildt, J.: The formation, properties and impact of secondary organic aerosol: Current and emerging issues, Atmos. Chem. Phys., 9, 5155–5236, 2009.

Hayes, P. L., Ortega, A. M., Cubison, M. J., Froyd, K. D., Zhao, Y., Cliff, S. S., Hu, W. W., Toohey, D. W., Flynn, J. H., Lefer, B. L., Grossberg, N., Alvarez, S., Rappenglück, B., Taylor, J. W., Allan, J. D., Holloway, J. S., Gilman, J. B., Kuster, W. C., de Gouw, J. A., Massoli, P., Zhang, X., Liu, J., Weber, R. J., Corrigan, A. L., Russell, L. M., Isaacman, G., Worton, D. R., Kreisberg, N. M., Goldstein, A. H., Thalman, R., Waxman, E. M., Volkamer, R., Lin, Y. H., Surratt, J. D., Kleindienst, T. E., Offenberg, J. H., Dusanter, S., Griffith, S., Stevens, P. S., Brioude, J., Angevine, W. M., and Jimenez, J. L.: Organic aerosol composition and sources in Pasadena, California, during the 2010 CalNex campaign, J. Geophys. Res., Atmos., 118, 9233–9257, 2013.

Huang, C., Hu, Q., Li, Y., Tian, J., Ma, Y., Zhao, Y., Feng, J., An, J., Qiao, L., Wang, H., Jing, S., Huang, D., Lou, S., Zhou, M., Zhu, S., Tao, S., and Li, L.: Intermediate volatility organic compound emissions from a large cargo vessel operated under real-world conditions, Environ. Sci. Technol., 52, 12934–12942, 2018.

Huang, D., Zhu, S., An, J., Wang, Q., Qiao, L., Zhou, M., He, X., Ma, Y., Sun, Y., Huang, C., Yu, J., and Zhang, Q.: Comparative assessment of cooking emission contributions to urban organic aerosol using online molecular tracers and aerosol mass spectrometry measurements, Environ. Sci. Technol., 55, 14526–14535, 2021.

Huang, L., Wang, Q., Wang, Y., Emery, C., Zhu, A., Zhu, Y., Yin, S., Yarwood, G., Zhang, K.,

https://doi.org/10.5194/acp-2022-268
Preprint. Discussion started: 28 April 2022


Atmospheric Chemistry and Physics Discussions

798 and Li, L.: Simulation of secondary organic aerosol over the Yangtze River Delta region:
799 The impacts from the emissions of intermediate volatility organic compounds and the SOA
800 modeling framework, Atmos. Environ., 246, 118079, 2021b.
801 Huang, R. J., Zhang, Y., Bozzetti, C., Ho, K., Cao, J., Han, Y., Daellenbach, K. R., Slowik, J.
802 G., Platt, S. M., Canonaco, F., Zotter, P., Wolf, R., Pieber, S. M., Bruns, E. A., Crippa, M.,
803 Ciarelli, G., Piazzalunga, A., Schwikowski, M., Abbaszade, G., Schnelle-Kreis, J.,
804 Zimmermann, R., An, Z., Szidat, S., Baltensperger, U., El Haddad, I., and Prévôt, A. S. H.:
805 High secondary aerosol contribution to particulate pollution during haze events in China,
806 Nature, 514, 218–222, 2014.
807 Huffman, J., Docherty, K., Mohr, C., Cubison, M., Ulbrich, I., Ziemann, P., Onasch, T., and
808 Jimenez, J.: Chemically-resolved volatility measurements of organic aerosol from
809 different sources, Environ. Sci. Technol., 43, 5351–5357, 2009.
810 Jathar, S. H., Gordon, T. D., Hennigan, C. J., Pye, H. O. T., Pouliot, G., Adams, P. J., Donahue,
811 N. M., and Robinson, A. L.: Unspeciated organic emissions from combustion sources and
812 their influence on the secondary organic aerosol budget in the United States, P. Natl. Acad.
813 Sci. USA, 111, 10473–10478, 2014.
814 Jimenez, J. L., Canagaratna, M. R., Donahue, N. M., Prevot, A. S. H., Zhang, Q., Kroll, J. H.,
815 DeCarlo, P. F., Allan, J. D., Coe, H., Ng, N. L., Aiken, A. C., Docherty, K. S., Ulbrich, I.
816 M., Grieshop, A. P., Robinson, A. L., Duplissy, J., Smith, J. D., Wilson, K. R., Lanz, V. A.,
817 Hueglin, C., Sun, Y. L., Tian, J., Laaksonen, A., Raatikainen, T., Rautiainen, J., Vaattovaara,
818 P., Ehn, M., Kulmala, M., Tomlinson, J. M., Collins, D. R., Cubison, M. J., Dunlea, J.,
819 Huffman, J. A., Onasch, T. B., Alfarra, M. R., Williams, P. I., Bower, K., Kondo, Y.,
820 Schneider, J., Drewnick, F., Borrmann, S., Weimer, S., Demerjian, K., Salcedo, D., Cottrell,
821 L., Griffin, R., Takami, A., Miyoshi, T., Hatakeyama, S., Shimono, A., Sun, J. Y., Zhang,
822 Y. M., Dzepina, K., Kimmel, J. R., Sueper, D., Jayne, J. T., Herndon, S. C., Trimborn, A.
823 M., Williams, L. R., Wood, E. C., Middlebrook, A. M., Kolb, C. E., Baltensperger, U., and
824 Worsnop, D. R.: Evolution of Organic Aerosols in the Atmosphere, Science, 326, 1525–
825 1529, 2009.

https://doi.org/10.5194/acp-2022-268
Preprint. Discussion started: 28 April 2022


Atmospheric Chemistry and Physics Discussions

826 Kim, D., Cho, C., Jeong, S., Lee, S., Nault, B. A., Campuzano-Jost, P., Day, D. A., Schroder, J.
827 C., Jimenez, J. L., Volkamer, R., Blake, D. R., Wisthaler, A., Fried, A., DiGangi, J. P.,
828 Diskin, G. S., Pusede, S. E., Hall, S. R., Ullmann, K., Gregory Huey, L., Tanner, D. J.,
829 Dibb, J., Knote, C. J., and Min, K., Field observational constraints on the controllers in
830 glyoxal (CHOCHO) reactive uptake to aerosol, Atmos. Chem. Phys., 22, 805–821, 2022.
831 Koo, B., Knipping, E., and Yarwood, G.: 1.5-Dimensional volatility basis set approach for
832 modeling organic aerosol in CAMx and CMAQ, Atmos. Environ., 95, 158–164, 2014.
833 Koss, A. R., Sekimoto, K., Gilman, J. B., Selimovic, V., Coggon, M. M., Zarzana, K. J., Yuan,
834 B., Lerner, B. M., Brown, S. S., Jimenez, J. L., Krechmer, J., Roberts, J. M., Warneke, C.,
835 Yokelson, R. J., and de Gouw, J.: Non-methane organic gas emissions from biomass
836 burning: identification, quantification, and emission factors from PTR-ToF during the
837 FIREX 2016 laboratory experiment, Atmos. Chem. Phys., 18, 3299–3319, 2018.
838 Li, J., Cao, L., Gao, W., He, L., Yan, Y., He, Y., Pan, Y., Ji, D., Liu, Z., and Wang, Y.: Seasonal
839 variations in the highly time-resolved aerosol composition, sources and chemical
840 processes of background submicron particles in the North China Plain, Atmos. Chem.
841 Phys., 21, 4521–4539, 2021.
842 Li, J., Han, Z., Li, J., Liu, R., Wu, Y., Liang, L., and Zhang, R.: The formation and evolution of
843 secondary organic aerosol during haze events in Beijing in wintertime, Sci. Total Environ.,
844 703, 134937, 2020.
845 Li, M., Zhang, Q., Kurokawa, J. i., Woo, J. H., He, K., Lu, Z., Ohara, T., Song, Y., Streets, D.
846 G., Carmichael, G. R., Cheng, Y., Hong, C., Huo, H., Jiang, X., Kang, S., Liu, F., Su, H.,
847 Zheng, B.: MIX: a mosaic Asian anthropogenic emission inventory under the international
848 collaboration framework of the MICS-Asia and HTAP. Atmos. Chem. Phys., 17, 935–963,
849 2017.
850 Li, Y., Ren, B., Qiao, Z., Zhu, J., Wang, H., Zhou, M., Qiao, L., Lou, S., Jing, S., Huang, C.,
851 Tao, S., Rao, P., and Li, J.: Characteristics of atmospheric intermediate volatility organic
852 compounds (IVOCs) in winter and summer under different air pollution levels, Atmos.
853 Environ., 210, 58–65, 2019.

https://doi.org/10.5194/acp-2022-268
Preprint. Discussion started: 28 April 2022


Atmospheric Chemistry and Physics Discussions

854 Li, Y. J., Sun, Y. L., Zhang, Q., Li, X., Li, M., Zhou, Z., and Chan, C. K.: Real-time chemical
855 characterization of atmospheric particulate matter in China: A review, Atmos. Environ.,
856 158, 270–304, 2017.
857 Liggio, J., Li, S., Hayden, K., Taha, Y. M., Stroud, C., Darlington, A., Drollette, B. D., Gordon,
858 M., Lee, P., Liu, P., Leithead, A., Moussa, S. G., Wang, D., Brien, J. O., Mittermeier, R.
859 L., Osthoff, H. D., Makar, P. A., Zhang, J., Brook, J. R., Lu, G., Staebler, R. M., Han, Y.,
860 Travis, W., Plata, D. L., and Gentner, D. R.: Oil sands operations as a large source of
861 secondary organic aerosols, Nature, 534, 1–16, 2016.
862 Lim, Y. B. and Ziemann, P. J.: Chemistry of secondary organic aerosol formation from OH
863 radical-initiated reactions of linear, branched, and cyclic alkanes in the presence of NO_x,
864 Aerosol Sci. Technol., 43, 604–619, 2009.
865 Liu, H., Man, H., Cui, H., Wang, Y., Deng, F., Wang, Y., Yang, X., Xiao, Q., Zhang, Q., Ding,
866 Y., and He, K.: An updated emission inventory of vehicular VOCs and IVOCs in China,
867 Atmos. Chem. Phys., 17, 12709–12724, 2017.
868 Liu, H., Meng, Z., Lv, Z., Wang, X., Deng, F., Liu, Y., Zhang, Y., Shi, M., Zhang, Q., and He,
869 K.: Emissions and health impacts from global shipping embodied in US–China bilateral
870 trade, Nat. Sustain., 2, 1027–1033, 2019.
871 Liu, Y., Li, L., An, J., Huang, L., Yan, R., Huang, C., Wang, H., Wang, Q., Wang, M., and Zhang,
872 W.: Estimation of biogenic VOC emissions and its impact on ozone formation over the
873 Yangtze River Delta region, China, Atmos. Environ., 186, 113–128, 2018.
874 Liu, Z., Gao, W., Yu, Y., Hu, B., Xin, J., Sun, Y., Wang, L., Wang, G., Bi, X., Zhang, G., Xu, H.,
875 Cong, Z., He, J., Xu, J., and Wang, Y.: Characteristics of PM2.5 mass concentrations and
876 chemical species in urban and background areas of China: emerging results from the
877 CARE-China network, Atmos. Chem. Phys., 18, 8849–8871, 2018.
878 Lu, Q., Murphy, B. N., Qin, M., Adams, P. J., Zhao, Y., Pye, H. O. T., Efstathiou, C., Allen, C.,
879 and Robinson, A. L.: Simulation of organic aerosol formation during the CalNex study:
880 Updated mobile emissions and secondary organic aerosol parameterization for
881 intermediate-volatility organic compounds, Atmos. Chem. Phys., 20, 4313–4332, 2020.

https://doi.org/10.5194/acp-2022-268
Preprint. Discussion started: 28 April 2022


Atmospheric Chemistry and Physics Discussions

882 Lu, Q., Zhao, Y., and Robinson, A. L.: Comprehensive organic emission profiles for gasoline,
883 diesel, and gas-turbine engines including intermediate and semi-volatile organic
884 compound emissions, Atmos. Chem. Phys., 18, 17637–17654, 2018.
885 May, A. A., Levin, E. J. T., Hennigan, C. J., Riipinen, I., Lee, T., Collett, J. L., Jimenez, J. L.,
886 Kreidenweis, S. M., and Robinson, A. L.: Gas-particle partitioning of primary organic
887 aerosol emissions: 3. Biomass burning, J. Geophys. Res.-Atmos., 118, 11327–11338, 2013.
888 McDonald, B. C., de Gouw, J. A., Gilman, J. B., Jathar, S. H., Akherati, A., Cappa, C. D.,
889 Jimenez, J. L., Lee-Taylor, J., Hayes, P. L., McKeen, S. A., Cui, Y. Y., Kim, S., Gentner,
890 D. R., Isaacman-VanWertz, G., Goldstein, A. H., Harley, R. A., Frost, G. J., Roberts, J. M.,
891 Ryerson, T. B., and Trainer, M.: Volatile chemical products emerging as largest
892 petrochemical source of urban organic emissions, Science, 359, 760–764, 2018.
893 Miao, R., Chen, Q., Shrivastava, M., Chen, Y., Zhang, L., Hu, J., Zheng, Y., and Liao, K.:
894 Process-based and observation-constrained SOA simulations in China: the role of
895 semivolatile and intermediate-volatility organic compounds and OH levels, Atmos. Chem.
896 Phys., 21, 16183–16201, 2021.
897 Ming, L., Jin, L., Li, J., Fu, P., Yang, W., Liu, D., Zhang, G., Wang, Z., and Li, X.: $PM_{2.5}$ in the
898 Yangtze River Delta, China: Chemical compositions, seasonal variations, and regional
899 pollution events, Environ. Pollut., 223, 200–212, 2017.
900 Murphy, B. N., Woody, M. C., Jimenez, J. L., Carlton, A. M. G., Hayes, P. L., Liu, S., Ng, N.
901 L., Russell, L. M., Setyan, A., and Xu, L.: Semivolatile POA and parameterized total
902 combustion SOA in CMAQv5.2: impacts on source strength and partitioning, Atmos.
903 Chem. Phys., 17, 11107–11133, 2017.
904 Nault, B. A., Jo, D. S., McDonald, B. C., Campuzano-Jost, P., Day, D. A., Hu, W., Schroder, J.
905 C., Allan, J., Blake, D. R., Canagaratna, M. R., Coe, H., Coggon, M. M., DeCarlo, P. F.,
906 Diskin, G. S., Dunmore, R., Flocke, F., Fried, A., Gilman, J. B., Gkatzelis, G., Hamilton,
907 J. F., Hanisco, T. F., Hayes, P. L., Henze, D. K., Hodzic, A., Hopkins, J., Hu, M., Huey, L.
908 G., Jobson, B. T., Kuster, W. C., Lewis, A., Li, M., Liao, J., Nawaz, M. O., Pollack, I. B.,
909 Peischl, J., Rappenglück, B., Reeves, C. E., Richter, D., Roberts, J. M., Ryerson, T. B.,

https://doi.org/10.5194/acp-2022-268
Preprint. Discussion started: 28 April 2022


Atmospheric Chemistry and Physics Discussions

910 Shao, M., Sommers, J. M., Walega, J., Warneke, C., Weibring, P., Wolfe, G. M., Young, D.
911 E., Yuan, B., Zhang, Q., de Gouw, J. A., and Jimenez, J. L.: Secondary organic aerosols
912 from anthropogenic volatile organic compounds contribute substantially to air pollution
913 mortality, Atmos. Chem. Phys., 21, 11201–11224, 2021.
914 Presto, A. A., Miracolo, M. A., Kroll, J. H., Worsnop, D. R., Robinson, A. L., and Donahue, N.
915 M.: Intermediate-volatility organic compounds: A potential source of ambient oxidized
916 organic aerosol, Environ. Sci. Technol., 43, 4744–4749, 2009.
917 Presto, A. A., Miracolo, M. A., Donahue, N. M., and Robinson, A. L.: Secondary organic
918 aerosol formation from high-NO_x photo-oxidation of low volatility precursors: n-alkanes,
919 Environ. Sci. Technol., 44, 2029–2034, 2010.
920 Presto, A. A., Nguyen, N. T., Ranjan, M., Reeder, A. J., Lipsky, E. M., Hennigan, C. J., Miracolo,
921 M. A., Riemer, D. D., and Robinson, A. L.: Fine particle and organic vapor emissions from
922 staged tests of an in-use aircraft engine, Atmos. Environ., 45, 3603–3612, 2011.
923 Qi, L., Liu, H., Shen, X., Fu, M., Huang, F., Man, H., Deng, F., Shaikh, A. A., Wang, X., Dong,
924 R., Song, C., and He, K.: Intermediate-volatility organic compound emissions from
925 nonroad construction machinery under different operation modes, Environ. Sci. Technol.,
926 53, 13832–13840, 2019.
927 Qi, L., Zhao, J., Li, Q., Su, S., Lai, Y., Deng, F., Man, H., Wang, X., Shen, X., Lin, Y., Ding, Y.,
928 and Liu, H.: Primary organic gas emissions from gasoline vehicles in China: Factors,
929 composition and trends, Environ. Pollut., 290, 117984, 2021.
930 Qin, M., Hu, A., Mao, J., Li, X., Sheng, L., Sun, J., Li, J., Wang, X., Zhang, Y., Hu, J.: $PM_{2.5}$
931 and O_3 relationships affected by the atmospheric oxidizing capacity in the Yangtze River
932 Delta, China, Sci. Total Environ., 810, 152268, 2022.
933 Ren, B., Zhu, J., Tian, L., Wang, H., Huang, C., Jing, S., Lou, S., An, J., Lu, J., Rao, P., Fu, Q.,
934 Huo, J., and Li, Y.: An alternative semi-quantitative GC/MS method to estimate levels of
935 airborne intermediate volatile organic compounds (IVOCs) in ambient air, Atmos.
936 Environ., X6, 100075, 2020.
937 Robinson, A. L., Donahue, N. M., Shrivastava, M. K., Weitkamp, E. A., Sage, A. M., Grieshop,

https://doi.org/10.5194/acp-2022-268
Preprint. Discussion started: 28 April 2022


Atmospheric Chemistry and Physics Discussions

938 A. P., Lane, T. E., Pierce, J. R., and Pandis, S. N.: Rethinking organic aerosols:
939 Semivolatile emissions and photochemical aging, Science, 315, 1259–1262, 2007.
940 Shrivastava, M. K., Cappa, C. D., Fan, J., Goldstein, A. H., Guenther, A. B., Jimenez, J. L.,
941 Kuang, C., Laskin, A., Martin, S. T., Ng, N. L., Petaja, T., Pierce, J. R., Rasch, P. J., Roldin,
942 P., Seinfeld, J. H., Shilling, J., Smith, J. N., Thornton, J. A., Volkamer, R., Wang, J.,
943 Worsnop, D. R., Zaveri, R. A., Zelenyuk, A., and Zhang, Q.: Recent advances in
944 understanding secondary organic aerosol: Implications for global climate forcing, Rev.
945 Geophys., 55, 509–559, 2017.
946 Sun, Y., Jiang, Q., Wang, Z., Fu, P., Li, J., Yang, T., and Yin, Y.: Investigation of the sources and
947 evolution processes of severe haze pollution in Beijing in January 2013, J. Geophys. Res.,
948 Atmos., 119, 4380–4398, 2014.
949 Tang, J., Li, Y., Li, X., Jing, S., Huang, C., Zhu, J., Hu, Q., Wang, H., Lu, J., Lou, S., Rao, P.,
950 and Huang, D.: Intermediate volatile organic compounds emissions from vehicles under
951 real world conditions, Sci. Total Environ., 788, 147795, 2021.
952 Tao, J., Zhang, L., Cao, J., and Zhang, R.: A review of current knowledge concerning $PM_{2.5}$
953 chemical composition, aerosol optical properties and their relationships across China,
954 Atmos. Chem. Phys., 17, 9485–9518, 2017.
955 Tkacik, D. S., Presto, A. A., Donahue, N. M., and Robinson, A. L.: Secondary organic aerosol
956 formation from intermediate-volatility organic compounds: Cyclic, linear, and branched
957 alkanes, Environ. Sci. Technol., 46, 8773–8781, 2012.
958 Tsimpidi, A. P., Karydis, V. A., Zavala, M., Lei, W., Molina, L., Ulbrich, I. M., Jimenez, J. L.,
959 and Pandis, S. N.: Evaluation of the volatility basis-set approach for the simulation of
960 organic aerosol formation in the Mexico City metropolitan area, Atmos. Chem. Phys., 10,
961 525–546, 2010.
962 US EPA: Final Report, SPECIATE Version 5.1, Database Development Documentation,
963 available at: https://www.epa.gov/air-emissions-modeling/speciate-51-and-50-addendum-
964 and-final-report (last access: 8 August 2021), 2021
965 Woody, M. C., Baker, K. R., Hayes, P. L., Jimenez, J. L., Koo, B., and Pye, H. O. T.:

https://doi.org/10.5194/acp-2022-268
Preprint. Discussion started: 28 April 2022


Atmospheric Chemistry and Physics Discussions

966 Understanding sources of organic aerosol during CalNex-2010 using the CMAQ-VBS,
967 Atmos. Chem. Phys., 16, 4081–4100, 2016.
968 Wu, L., Ling, Z., Liu, H., Shao, M., Lu, S., Wu, L., and Wang, X.: A gridded emission inventory
969 of semi-volatile and intermediate volatility organic compounds in China, Sci. Total
970 Environ., 761, 143295, 2021.
971 Wu, L., Wang, X., Lu, S., Shao, M., and Ling, Z.: Emission inventory of semi-volatile and
972 intermediate-volatility organic compounds and their effects on secondary organic aerosol
973 over the Pearl River Delta region, Atmos. Chem. Phys., 19, 8141–8161, 2019.
974 Xu, L., Guo, H., Boyd, C. M., Klein, M., Bougiatioti, A., Cerully, K. M., Hite, J. R., Isaacman-
975 VanWertze, G., Kreisberg, N. M., Knote, C., Olson, K., Koss, A., Goldstein, A. H., Hering,
976 S. V., de Gouw, J., Baumann, K., Lee, S., Nenes, A., Weber, R. J., and Ng, N. L.: Effects
977 of anthropogenic emissions on aerosol formation from isoprene and monoterpenes in the
978 southeastern United States, P. Natl. Acad. Sci. USA, 112, 37–42, 2015.
979 Yang, W., Li, J., Wang, W., Li, J., Ge, M., Sun, Y., Chen, X., Ge, B., Tong, S., Wang, Q., and
980 Wang, Z.: Investigating secondary organic aerosol formation pathways in China during
981 2014, Atmos. Environ., 213, 133–147, 2019.
982 Yao, T., Li, Y., Gao, J., Fung, J. C. H., Wang, S., Li, Y., Chan, C. K., and Lau, A. K. H.: Source
983 apportionment of secondary organic aerosols in the Pearl River Delta region: Contribution
984 from the oxidation of semi-volatile and intermediate volatility primary organic aerosols,
985 Atmos. Environ., 222, 117111, 2020.
986 Yu, K., Zhu, Q., Du, K., and Huang, X.: Characterization of nighttime formation of particulate
987 organic nitrates based on high-resolution aerosol mass spectrometry in an urban
988 atmosphere in China, Atmos. Chem. Phys., 19, 5235–5249, 2019.
989 Yuan, B., Shao, M., Lu, S., and Wang, B.: Source profiles of volatile organic compounds
990 associated with solvent use in Beijing, China, Atmos. Environ., 44, 1919–1926, 2010.
991 Zhang, H, Yee, L. D., Lee, B. H., Curtis, M. P., Worton, D. R., Isaacman-VanWertz, G.,
992 Offenberg, J. H., Lewandowski, M., Kleindienst, T. E., Beaver, M. R., Holder, A. L.,
993 Lonneman, W. A., Docherty, K. S., Jaoui, M., Pye, H. T. O., Hu, W., Day, D. A.,

https://doi.org/10.5194/acp-2022-268
Preprint. Discussion started: 28 April 2022


Atmospheric Chemistry and Physics Discussions

994 Campuzano-Jost, P., Jimenez, J. L., Guo, H., Weber, R. J., de Gouw, J., Koss, A. R.,
995 Edgerton, E. S., Brune, W., Mohr, C., Lopez-Hilfiker, F. D., Lutz, A., Kreisberg, N. M.,
996 Spielman, S. R., Hering, S. V., Wilson, K. R., Thornton, J. A., and Goldstein, A. H.:
997 Monoterpenes are the largest source of summertime organic aerosol in the southeastern
998 United States, P. Natl. Acad. Sci. USA, 115, 2038–2043, 2018.
999 Zhang, Q., Jimenez, J. L., Canagaratna, M. R., Allan, J. D., Coe, H., Ulbrich, I., Alfarra, M. R.,
1000 Takami, A., Middlebrook, A. M., Sun, Y. L., Dzepina, K., Dunlea, E., Docherty, K.,
1001 DeCarlo, P. F., Salcedo, D., Onasch, T., Jayne, J. T., Miyoshi, T., Shimono, A., Hatakeyama,
1002 S., Takegawa, N., Kondo, Y., Schneider, J., Drewnick, F., Borrmann, S., Weimer, S.,
1003 Demerjian, K., Williams, P., Bower, K., Bahreini, R., Cottrell, L., Griffin, R. J., Rautiainen,
1004 J., Sun, J. Y., Zhang, Y. M., and Worsnop, D. R.: Ubiquity and dominance of oxygenated
1005 species in organic aerosols in anthropogenically-influenced Northern Hemisphere
1006 midlatitudes, Geophys. Res. Lett., 34, L13801, 2007.
1007 Zhang, Y., Vijayaraghavan, K., and Seigneur, C.: Evaluation of three probing techniques in a
1008 three-dimensional air quality model, J. Geophys. Res., Atmos., 110, D02305, 2005.
1009 Zhao, B., Wang, S., Donahue, N. M., Jathar, S. H., Huang, X. F., Wu, W., Hao, J., and Robinson,
1010 A. L.: Quantifying the effect of organic aerosol aging and intermediate-volatility emissions
1011 on regional scale aerosol pollution in China, Sci. Rep., 6, 28815, 2016a.
1012 Zhao, Y., Hennigan, C. J., May, A. A., Tkacik, D. S., De Gouw, J. A., Gilman, J. B., Kuster, W.
1013 C., Borbon, A., and Robinson, A. L.: Intermediate-volatility organic compounds: A large
1014 source of secondary organic aerosol, Environ. Sci. Technol., 48, 13743–13750, 2014.
1015 Zhao, Y., Kreisberg, N. M., Worton, D. R., Isaacman, G., Weber, R. J., Liu, S., Day, D. A.,
1016 Russell, L. M., Markovic, M. Z., VandenBoer, T. C., Murphy, J. G., Hering, S. V., and
1017 Goldstein, A. H.: Insights into secondary organic aerosol formation mechanisms from
1018 measured gas/particle partitioning of specific organic tracer compounds, Environ. Sci.
1019 Technol., 47, 3781−3787, 2013.
1020 Zhao, Y., Nguyen, N. T., Presto, A. A., Hennigan, C. J., May, A. A., and Robinson, A. L.:
1021 Intermediate volatility organic compound emissions from on-road diesel vehicles:

https://doi.org/10.5194/acp-2022-268
Preprint. Discussion started: 28 April 2022


Atmospheric Chemistry and Physics Discussions

1022 Chemical composition, emission Factors, and estimated secondary organic aerosol
1023 production, Environ. Sci. Technol., 49, 11516–11526, 2015.
1024 Zhao, Y., Nguyen, N. T., Presto, A. A., Hennigan, C. J., May, A. A., and Robinson, A. L.:
1025 Intermediate Volatility Organic Compound Emissions from On-Road Gasoline Vehicles
1026 and Small Off-Road Gasoline Engines, Environ. Sci. Technol., 50, 4554–4563, 2016b.
1027 Zhu, S., Wang, Q., Qiao, L., Zhou, M., Wang, S., Lou, S., Huang, D., Wang, Q., Jing, S., Wang,
1028 H., Chen, C., Huang, C., and Yu, J. Z.: Tracer-based characterization of source variations
1029 of $PM_{2.5}$ and organic carbon in Shanghai influenced by the COVID-19 lockdown, Faraday
1030 Discuss., 226, 112, 2021.
1031 Zhu, W., Zhou, M., Cheng, Z., Yan, N., Huang, C., Qiao, L., Wang, H., Liu, Y., Lou, S., and
1032 Guo, S.: Seasonal variation of aerosol compositions in Shanghai, China: Insights from
1033 particle aerosol mass spectrometer observations, Sci. Total Environ., 771, 144948, 2021.
1034